DEPARTMENT OF ELECTRICAL
ENGINEERING
INDIAN INSTITUTE OF TECHNOLOGY
MADRAS
CHENNAI - 600036

Control Strategy for a Small-Scale Microgrid Based on Battery Energy Storage System

A Project Report

Submitted by

PRANIT GHARATKAR

In the partial fulfilment of requirements

For the award of the degree

Of

MASTER OF TECHNOLOGY

Jun 2022

DEPARTMENT OF ELECTRICAL
ENGINEERING
INDIAN INSTITUTE OF TECHNOLOGY
MADRAS
CHENNAI - 600036

Control Strategy for a Small-Scale Microgrid Based on Battery Energy Storage System

A Project Report

Submitted by

PRANIT GHARATKAR

In the partial fulfilment of requirements

For the award of the degree

Of

MASTER OF TECHNOLOGY

Jun 2022

CERTIFICATE

This is to undertake that the Thesis (or Project report) titled **CONTROL STRATEGY FOR A SMALL-SCALE MICROGRID BASED ON BATTERY ENERGY STORAGE SYSTEM**, submitted by me to the Indian Institute of Technology Madras, for the award of M Tech, is a bona fide record of the research work done by me under the supervision of **Dr. Mrs. LAKSHMINARASAMMA N**. The contents of this Thesis (or Project report), in full or in parts, have not been submitted to any other Institute or University for the award of any degree or diploma.

Place: Chennai 600 036

Date: Jun 2022

PRANIT GHARATKAR

Research Scholar

Dr. Mrs. LAKSHMINARASAMMA N

Research Guide

ACKNOWLEDGEMENTS

We take this opportunity to express our heartfelt gratitude towards our professor and project guide **Dr. Mrs. LAKSHMINARASAMMA N**, Professor, EED, IIT Madras for her valuable guidance and supervision. We thank her for her constant support throughout both the project phases.

We express our gratitude towards **Dr. R. DAVID KOILPILLAI** , HOD and Professor, EED, IIT Madras, for always helping and motivating us in every way possible.

We would also like to express our humble and sincere thanks to **NITHEESH Sir** without whom this project would not have been materialized.

We also thank everyone else who directly or indirectly have contributed in the completion of this project. Their contribution has been a vital input.

Pranit Gharatkar

ABSTRACT

As the concept of zero carbon has been introduced, the traditional fossil fuel based electrical power generation units will have limited application in future. Across the world, the coal based thermal power plants are replaced by natural gas based power plant in order to handle the carbon exposure to the environment, But on other hand natural gas based power plants are costlier as the production of natural gas is limited.

One of the feasible solution is to use available renewable resources. Nowadays, the PV system has wide application but it has one disadvantage as the weather conditions affects its performance. In this thesis we have discussed the PV and battery based microgrid system where battery acts as primary backup whenever the PV system unable to perform well. Microgrid can run in either grid-connected mode or off-grid-connected mode. Both of these modes are explained using mathematical models.

This thesis focuses on the modeling and control of the PV and battery energy storage system and the proposed model and control technique is verified using MATLAB/Simulink.

TABLE OF CONTENTS

LIST OF TABLES

LIST OF FIGURES

CHAPTER 1

MICROGRID SYSTEM

The commonly used fuels for the generation of electricity are fossil fuels (e.g. coal, petroleum, natural gas) but due to limited availability it is important to find out alternatives. Renewable energy especially solar and wind have become most popular sources as they are available most of the time.

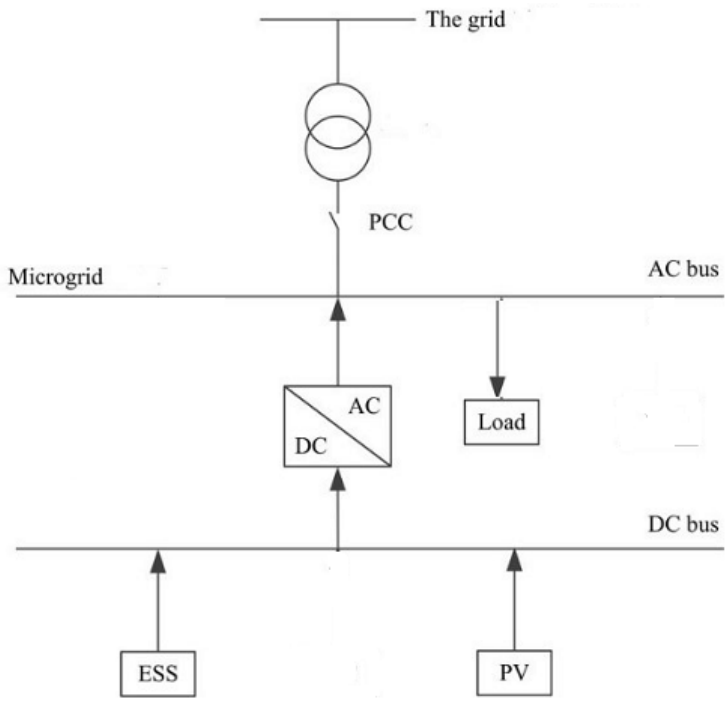

Fig. 1.1: General Structure of Microgrid

The electricity produced by such resources have less voltage level as well as they work for low power rating because of the initial cost and other factors. However, if we integrate such small units to form a small grid which can be connected with the main power grid then the system can be more economical and at peak hours. They can even handle power demand efficiently which brought the concept of microgrid. Figure 1.1 shows a general structure of a microgrid which consists of DGs (distributed generators), DC bus, AC bus, Converters and main power grid. (Keyhani and Marwali, 2011)

1.1 STORAGE SYSTEM IN MICROGRID

In energy management system of the microgrid, the storage plays a significant role in achieving the power balance between the renewable source, local loads and the utility grid. The storage serves primary backup for such system. In Appendix A different storage systems are described.(Ashok Jhunjhunwala, 2021)

- Day by day the energy density increases with reduction in cost, the batteries are predominantly used to store electrical energy.
- Supercapacitors are also used where they have moderate energy density.
- Their ratings are chosen based on the applications of the microgrid.

1.2 POWER CONVERTER

Voltage source converter (VSC) acts as a interface in between microgrid and load, microgrid and main grid.

Table 1.1: Power Converter Classification based on Voltage Profile

DC - DC Converter	DC - AC / AC - DC Converter
• They are normally used for step up or step down the voltage level. • Active Power is shared. DC / Real Power Sharing. • DC loads / storage system requires such converter.	• They are normally used for inverter / rectifier operation. • Apparent power is shared with specified voltage and frequency. • AC / DC loads requires such converter.

It can be categories as shown in Table 1.1 and they also serve following objectives

- Compensation of current harmonics
- Load balancing
- Reactive power support

1.3 CLASSIFICATION OF GRID BASED OPERATION MODES

The classification is done as per fluctuations in voltage and frequency. From Figure 1.2 it is well illustrated that if the voltage and frequency both are in within limits (w.r.t grid specifications) then the system will operate as grid connected mode (grid interactive mode) else it will be in standalone mode (islanded mode). In addition to that, in grid connected mode VSC (inverter) will operate in current controlled mode and in islanded mode VSC (inverter) will operate in voltage controlled mode. For permissible tolerance value in frequency specification $(f_{g,min} < f_g < f_{g,max})$, under grid interactive mode microgrid will operate in three different modes.(Gao, 2019)

where,

f_g : operating frequency of microgrid

$f_{g,o}$: nominal frequency of microgrid

$f_{g,min}$: minimum frequency allowed for grid interactive mode

$f_{g,max}$: maximum frequency allowed for grid interactive mode

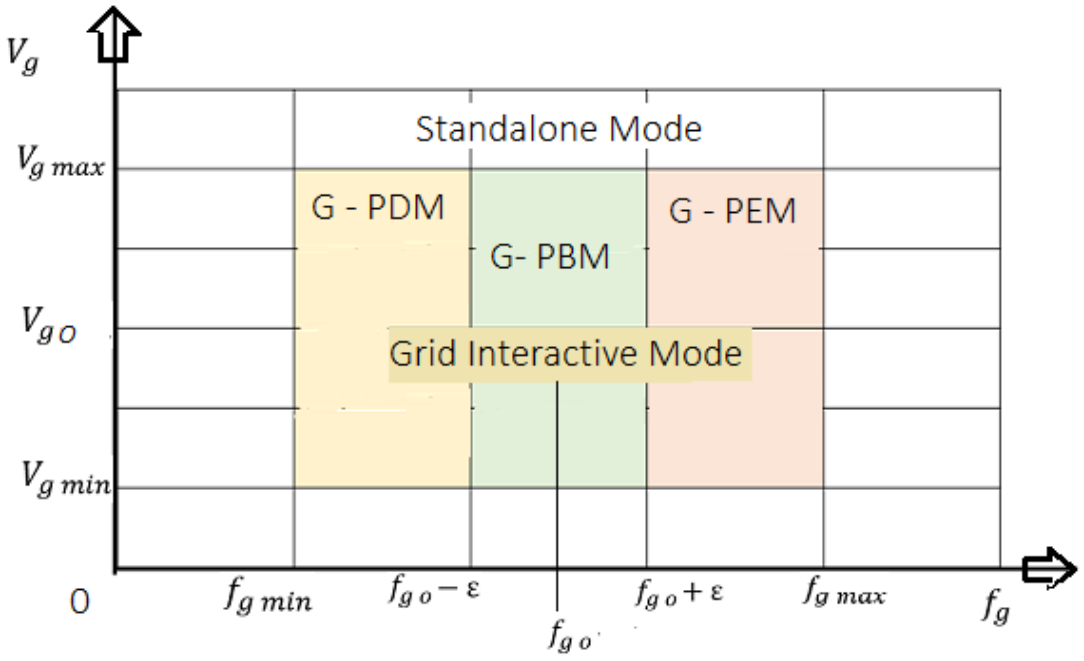

Fig. 1.2: Classification of Grid Based Operating Modes

Further, for very small deviation $'\epsilon'$ w.r.t to nominal frequency $f_{g,o}$ a new frequency band is proposed such as $f^{'}_{g,min} = f_{g,o} - \epsilon$, $f^{'}_{g,max} = f_{g,o} + \epsilon$. This is done using numerical methods and for this frequency band the three modes are named as

- grid power excess mode $(G-PEM)$ where $f^{'}_{g,max} < f_g < f_{g,max}$, for such zone the microgrid can deliver power to grid more than what grid has demanded at that instant.
- grid power balance mode $(G - PBM)$ where $f^{'}_{g,min} < f_g < f^{'}_{g,max}$, for such zone the microgrid has ability to match the grid demand at that instant.
- grid power deficit mode $(G - PBM)$ where $f_{g,min} < f_g < f^{'}_{g,min}$, for such zone the microgrid would deliver less power to grid demand.

The above three modes can be explained using the induction machine used in wind power system connected to grid where following equations are helpful.

Slip, $s = (n_s - n_r)/(n_s)$

Rotor power, $P_r = -sP_s$ ..... (taking grid power as reference)

Grid power, $P_g = P_s + P_r$

n_s : synchronous speed

n_r : rotor speed

P_s : stator power

Table 1.2: Power Flow in Wind Power System under Grid Connected Mode

	Super Synchronous Speed $(n_r > n_s)$	Synchronous Speed $(n_r = n_s)$	Sub Synchronous Speed $(n_r < n_s)$
Power Flow	Both stator and rotor gives real power to grid	Only stator gives power to grid	Stator gives real power to grid whereas rotor takes power from grid

The above behaviour of induction machine used in wind power system explained in Table 1.2 can be observed for the frequency band $f_{g,min} < f_g < f_{g,max}$.

1.4 STAGES OF CONTROLLERS IN MICROGRID

Figure 1.3 represents typical schematic of controller stages in microgrid system. The primary controller near DC bus ensures constant voltage, the secondary controller near AC bus ensures rated voltage at power frequency and the tertiary controller controls the power flow. The components along with control strategies are explained in Chapter 2. (Gao, 2019)

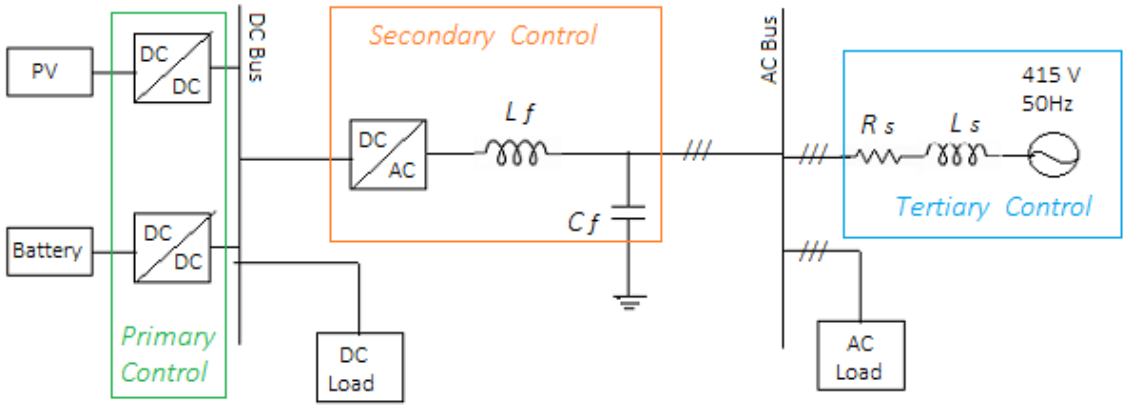

Fig. 1.3: Stages of Controllers in Microgrid

1.5 CONTROL STRATEGIES OF MICROGRID

1.5.1 Master-Slave Control

In islanded mode, master DGs decides the nominal voltage and frequency, and all other DGs use constant power control based on this specific voltage and frequency. The structure of this mode is shown in Figure 1.4.

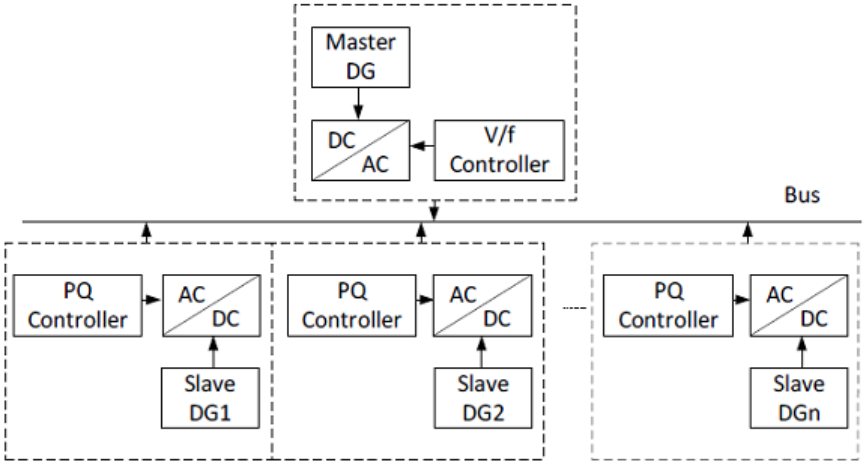

Fig. 1.4: Master Slave Control

1.5.2 Peer to Peer Control

In this mode, DGs are equal, so there is no master and slave anymore. Each DG controls its voltage and frequency based on the information from the common bus. The most common controller for them is Droop Controller, which can change their own power to share the loads based on different droop-coefficients. For different load curves different droop-coefficients are examined and from there the voltage and frequency proportional to droop-coefficients are set. The structure of this mode is shown in Figure 1.5.

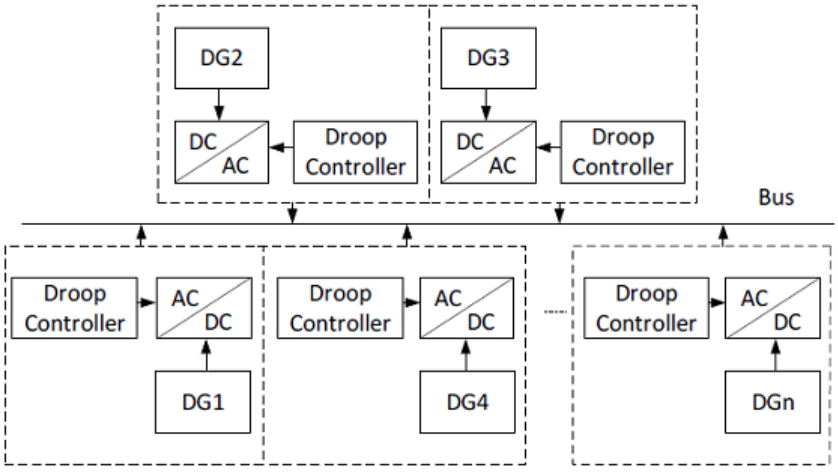

Fig. 1.5: Peer to Peer Control

1.6 SOLAR CELL

Solar cell operation is based on the photovoltaic effect where solar energy is converted from solar to electrical. The solar cell is basically a PV module made up of special p-n junction semiconductor device. Whenever, the light falls on solar cell such that the potential across the p-n junction exceeds its threshold value current starts flowing through device due to formation of minority carriers (free electron-hole pair) in the device.

Since the PV cell is made up of semiconductor device who's I-V characteristic is similar to that of p-n junction diode where the physical structure decides the behaviour of plot and most of the semiconductors have a non-linear I-V curve. Due to non-linearity of I-V and P-V characteristics under variable irradiance and temperature, usually it needs to linearized while studying dynamic model of such semiconductor device. Figure 1.6 shows equivalent electrical mathematical model (practical), the configuration is known as two diode model that give more details about the dynamics of the device.

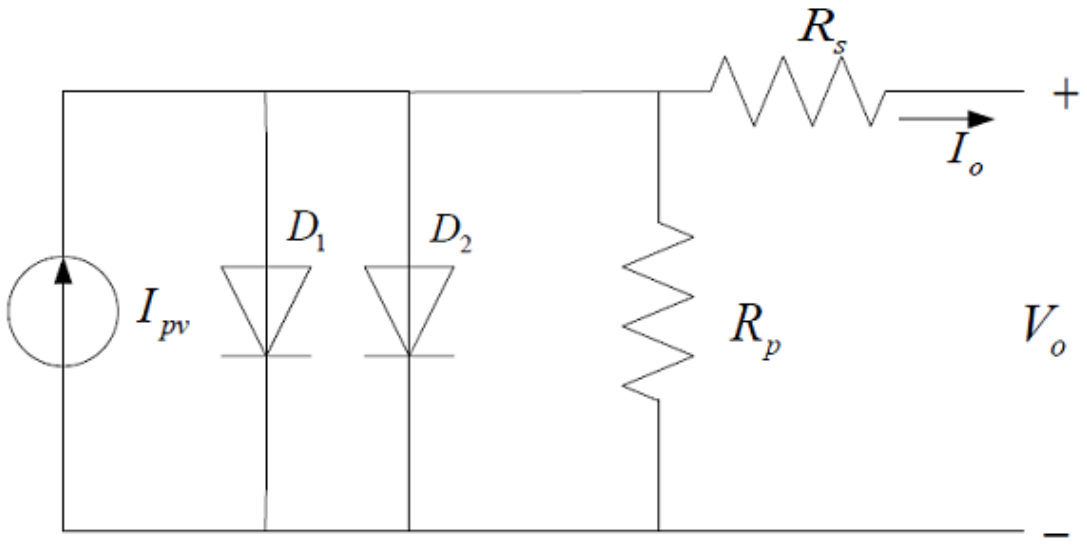

Fig. 1.6: Two Diode Model of PV Cell

For single p-n junction diode the relationship between current, voltage and temperature is given by equation 1.1. Further, the influence of irradiance and temperature on photocurrent can be describe by equation 1.2. Also, equation 1.3 gives relationship between diode reverse saturation current and the cell temperature.

$$I_o = I_{pv} - I_s[\exp(\frac{q\ \ (V_o + I_o R_s)}{k\ \ T_c\ \ A}) - 1] \tag{1.1}$$

$$I_{pv} = I_{sc} + K_t(T_c - T_o)H \tag{1.2}$$

$$I_s = I_{rs}(T_c/T_o)^3[\exp(\frac{q\ E_g\ (\frac{1}{T_o} - \frac{1}{T_c})}{k\ A})] \tag{1.3}$$

where,

I_o : output current

I_{pv} : photocurrent of PV cell

I_s : diode reverse saturation current

q : electron charge ($q = 1.6910^{-19}\ C$)

V_o : output voltage

T_c : temperature of PV cell in $Kelvin$

k : Boltzmann's constant ($k = 1.3810^{-23}\ J/K$)

A : ideal factor ($1\ for\ Ge\ and\ 2\ for\ Si$)

I_{sc} : short circuit current of cell at $T_o = 25°C$ and $H = 1kW/m^2$

K_t : temperature coefficient of short circuit current

H : solar irradiance in kW/m^2

I_{rs} : reverse saturation current of cell at $T_o = 25°C$ and $H = 1kW/m^2$

E_g : band gap energy for the semiconductor device

From above discussion, the mathematical description for two diode model can be obtained as,

$$I_o = I_{pv} - I_{s1}[\exp(\frac{q\ (V_o+I_oR_s)}{k\ T_c\ A}) - 1] - I_{s2}[\exp(\frac{q\ (V_o+I_oR_s)}{k\ T_c\ A}) - 1]$$

$$- \frac{(V_o + I_oR_s)}{R_p} \tag{1.4}$$

where,

I_{s1} : diode $D_1's$ reverse saturation current

I_{s2} : diode $D_2's$ reverse saturation current

As the power output of a single PV cell is very less and to full-fill the requirement, multiple PV cells can be assembled in parallel as well as in series configuration to form a PV module / PV array which also helps us to raise the voltage level of PV system and also current sharing capability. The typical structure is shown in Figure 1.7 and the mathematical description can be explained using equation 1.5.

$$I_o = N_pI_{pv} - N_pI_{s1}[\exp(\frac{q\ (N_p\ V_o\ +\ N_s\ I_oR_s)}{N_p\ N_s\ k\ T_c\ A}) - 1] - N_pI_{s2}[\exp(\frac{q\ (N_p\ V_o\ +\ N_s\ I_oR_s)}{N_p\ N_s\ k\ T_c\ A}) - 1]$$

$$- \frac{(N_p\ V_o + N_s\ I_oR_s)}{N_s\ R_p} \tag{1.5}$$

where,

N_p : number of cells connected in parallel

N_s : number of cells connected in series

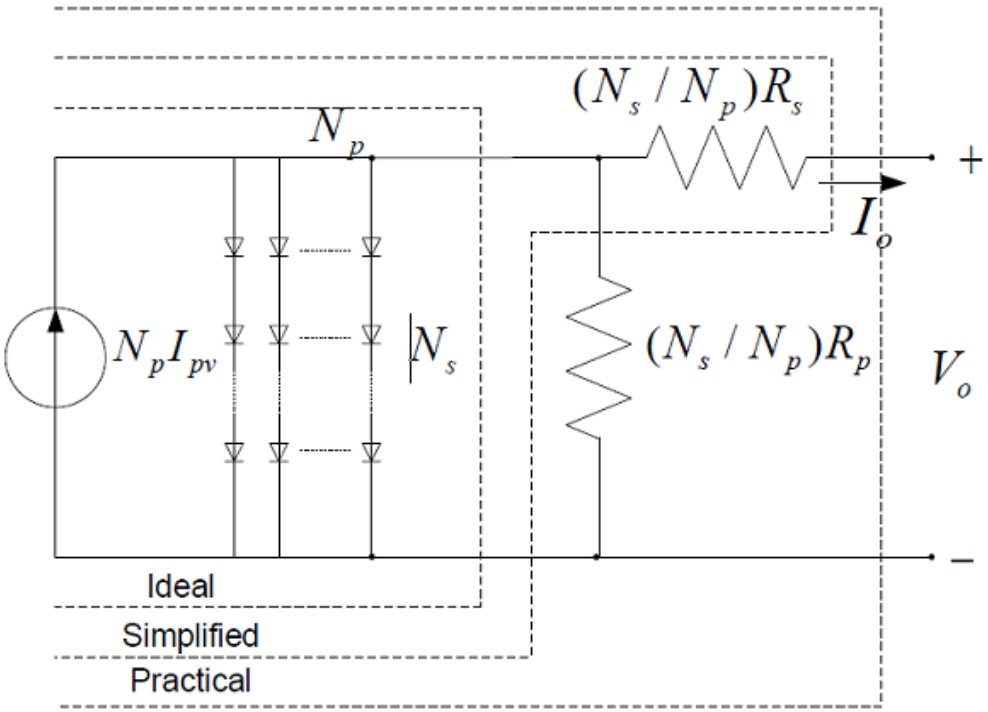

Fig. 1.7: PV Module

Using equations 1.1 to 1.5 the I-V characteristics can be studied.

- Short Circuit Current : $I_{sc} = I|_{V=0}$
  - > Terminal Current is equal to I_{pv}
  - > Diodes are not biased
  - > I_{sc} is proportional to irradiance
  - > Dependence of I_{sc} on temperature is negligible

- Open Circuit Voltage : $V_{oc} = V|_{I=0}$
  - > I_{pv} completely flows through diodes
  - > Diodes are directly biased

$$V_{oc} = \frac{2}{3}\frac{k\,T}{q} ln \frac{I_{sc} + I_{s1} + I_{s2}}{I_{s1}\,I_{s2}} \approx \frac{2}{3}\frac{k\,T}{q} ln \frac{I_{sc}}{I_{s1}\,I_{s2}} \tag{1.6}$$

  - > V_{oc} has logarithmic dependence on irradiance
  - > Temperature effect on V_{oc} is noticeable

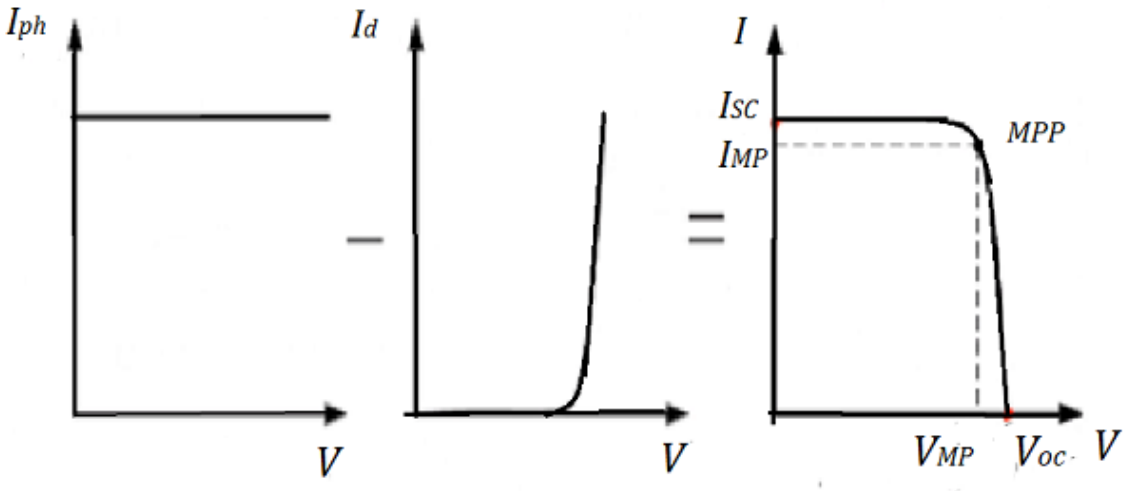

Fig. 1.8: I-V Characteristics of PV Cell

1.7 MAXIMUM POWER POINT TRACKING

As discussed in Section 1.6, the output power is primarily dependent on circuit structure, solar radiation and temperature. In order to operate a PV system in optimized way maximum power point tracking (MPPT) is necessary. Operating point depends on the PV characteristics and load line. Operating point can be altered by altering the load line seen from the PV panel. Usually, a power interface (buck/boost converter) is used. To achieve MPPT, several algorithms have been proposed out of which the $Perturb\ \&\ Observe\ Method$ and the $Incremental\ Conductance\ Method$ are two of the popular methods widely used. Equation 1.7 is the condition for maximum power.

$$\frac{d\,P}{d\,V} = \frac{d\,(V\,I)}{d\,V}|_{V=\,V_{MP}} = (I\ +\ V\,\frac{d\,I}{d\,V})|_{V=\,V_{MP}} = 0 \tag{1.7}$$

$$\eta = FF\,\frac{V_{oc}\,I_{sc}}{P_i} \tag{1.8}$$

$$FF = \frac{V_{MP} \star I_{MP}}{V_{oc} \star I_{sc}} \tag{1.9}$$

where,

η : PV cell efficiency

FF : Fill Factor, for ideal case $FF = 1$

V_{MP} : voltage at maximum power point

I_{MP} : current at maximum power point

P_i : input power

1.7.1 *Perturb and Observe Method*

The principle of this technique is to perturb PV module operating voltage periodically with a small increment, then observe the change direction of the output power so that the further control signal can be determined. This method is easy for implantation but it has one drawback that oscillations occurs nearby operating point. Figure 1.9 represents the schematic of algorithm where " i " is present state and " d " is step size of working voltage.

1.7.2 *Incremental Conductance Method*

The incremental conductance method is similar to as that of perturb and observe method but here oscillations around operating point would be significantly lower. The algorithm is represented in Figure 1.10.

Using equation 1.7, $I + V\frac{d\,I}{d\,V} = 0$ can be linearized as,

$$I + V\frac{\Delta\,I}{\Delta\,V} = 0 \tag{1.10}$$

where,

$\Delta\,I$: small increment in current

$\Delta\,V$: small increment in voltage

$\frac{\Delta\,I}{\Delta\,V}$: incremental conductance

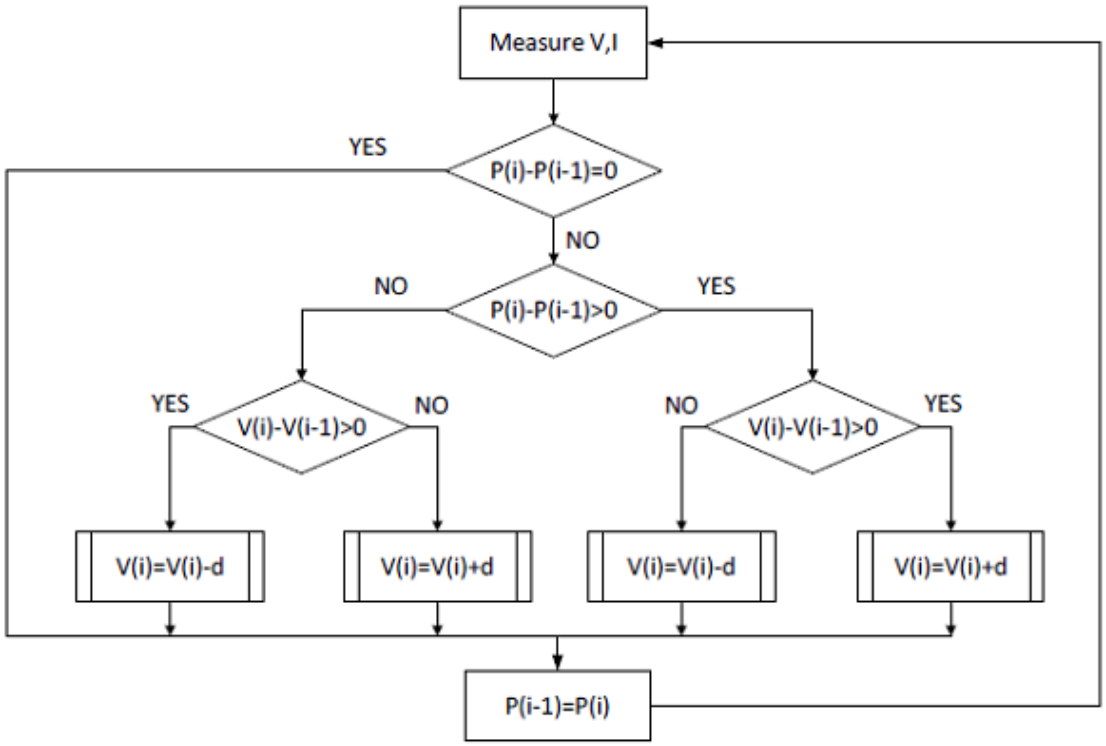

Fig. 1.9: Perturb and Observe Algorithm

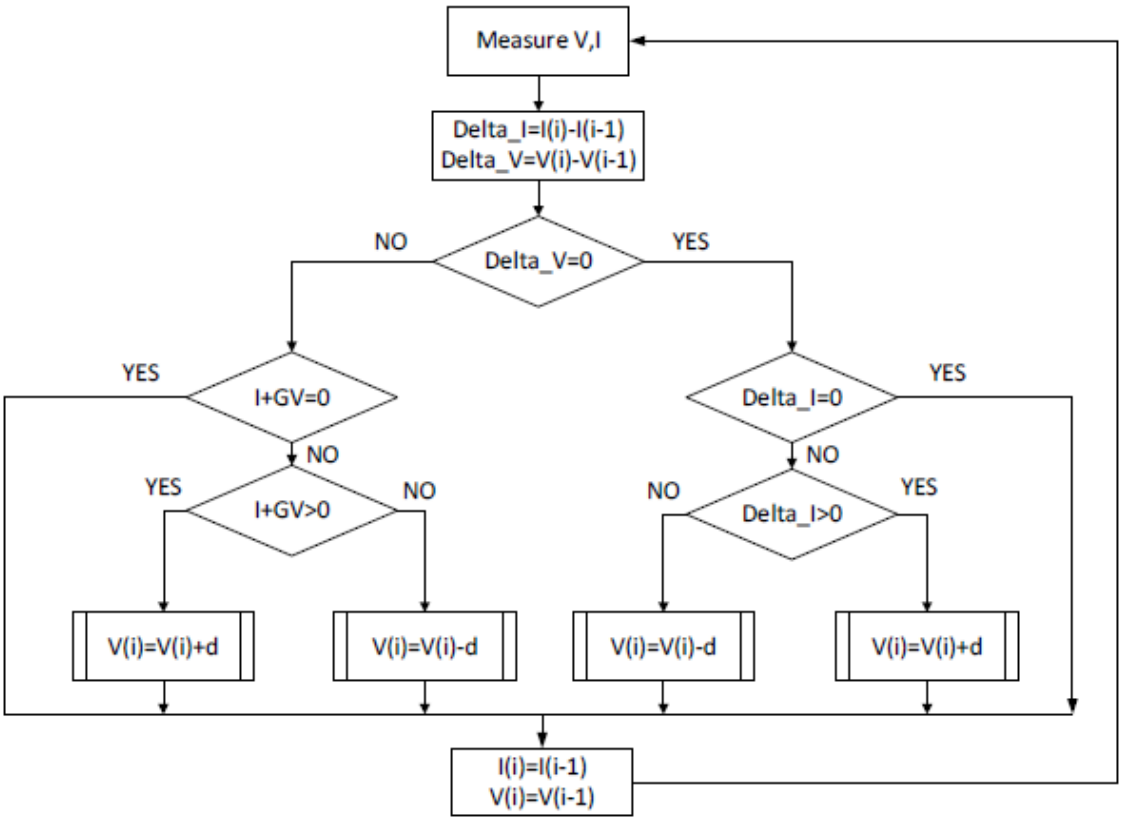

Fig. 1.10: Incremental Conductance Method

CHAPTER 2

PV SYSTEM CONTROL

Figure 2.1 represents the schematic of control stages, the first stage (DC-DC Control) ensures regulated output voltage along with MPPT . In second stage (DC-AC Control or Inverter Control) the DC voltage is converted to AC voltage (three phase) at power frequency and power is controlled at this stage. (Shen, 2017) (Patel, 2018)

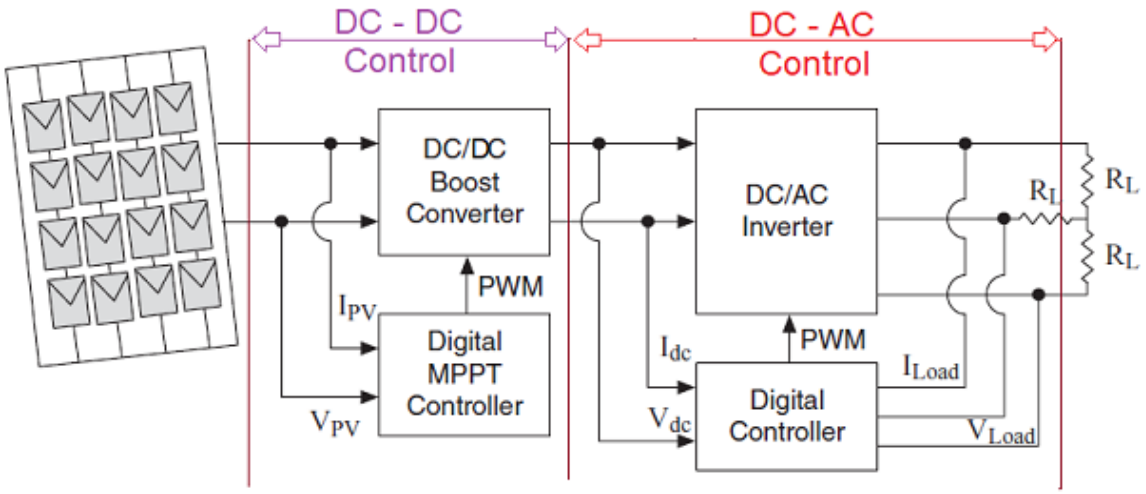

Fig. 2.1: Control Stages in PV System

2.1 DC-DC CONTROLLER OF PV SYSTEM

The DC-DC Controller can step-up or step-down DC voltage as per application. Figure 2.2 shows typical controller scheme of step-up converter where the inner loop is known as the current-controlled loop and the outer loop is known as voltage-controlled loop. Voltage controller loop controls the PV voltage and the reference voltage $v_{pv,ref}$ can be obtained using MPPT algorithm. The " K_v " and " K_i " are derivative constants which are added in voltage and current loop respectively to improve dynamic response of the controller. (Blaabjerg, 2018)

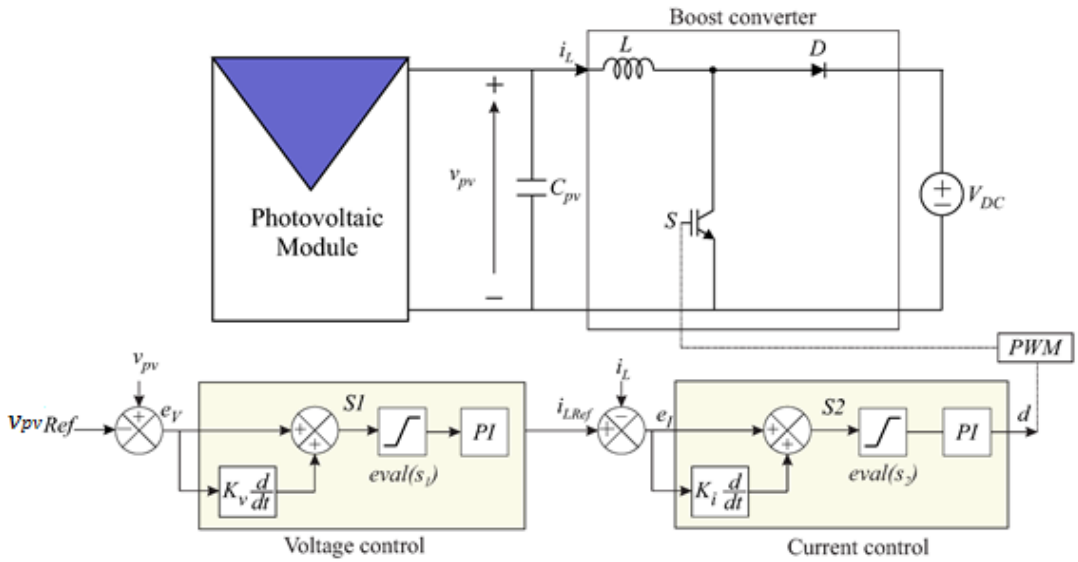

Fig. 2.2: DC-DC Controller Structure

Current controlled loop regulates the inductor current and the reference current "$i_{L,ref}$" is given by

$$i_{L,ref} = K_{p,v} \left(v_{pv,ref} - v_{pv} \right) + K_{i,v} \int \left(v_{pv,ref} - v_{pv} \right) dt \tag{2.1}$$

where,

$K_{p,v}$: proportional constant for voltage loop

$K_{i,v}$: proportional constant for voltage loop

Several types of DC-DC converters are available and the approach for controller design would be similar as explained above.

i Buck-Boost converter (inverted output)

ii Cuk converter (output is similar to buck-boost but current ripple is less)

iii SEPIC converter (non-inverted output but has ripple in current profile)

iv Zeta (output is similar to SEPIC but current ripple is less)

v SEPIC-Zeta (bidirectional converter)

2.2 INVERTER CONTROLLER OF PV GRID-CONNECTED SYSTEM

Figure 2.3 shows the control structure of inverter controller. It has two loop as inner loop and outer loop. The output loop is known as voltage loop and it is slower than inner loop as the state space variables are associated filter capacitor. The inner loop is known as current loop and it is faster than outer loop. The outer loop ensures that system has matched the desired output voltage/power and the inner loop ensures the stability of system as net load current changes with change in load.

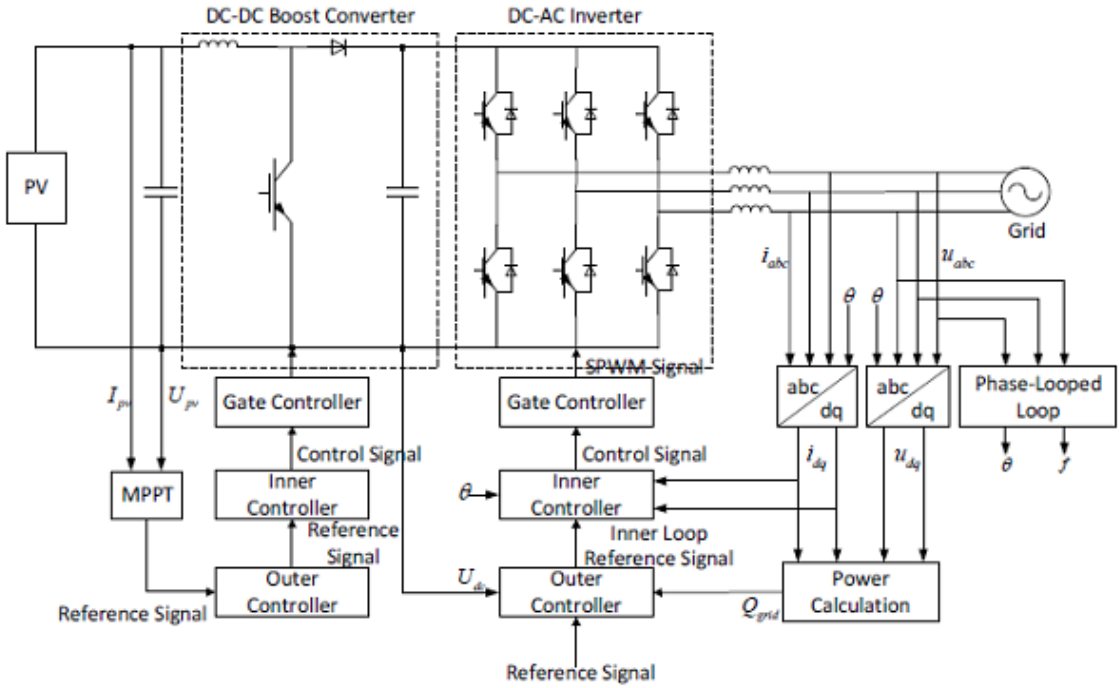

Fig. 2.3: Inverter Controller of PV Grid-Connected System

When microgrid operates in islanded mode then $Droop\ Control\ Technique$ is used which gives constant voltage. And when microgrid operates in grid connected mode then $P - Q\ Control\ Technique$ is used which gives constant power. In this thesis we have initially focused on modelling and analysis of grid connected mode operation using state space model by applying simple Kirchhoff's law used in electrical system. Further, the same model has been extended to derive the system, grid operating under standalone mode (islanded mode).

2.3 P-Q CONTROL TECHNIQUE

Here, the active (P) and reactive (Q) power are controlled to follow reference power. The control strategy explained in this thesis is based on decoupling d-q variables using synchronous reference frame phase locked loop model. Equation 2.2 describe the power in d-q reference using reference transformation theory explained in Appendix C. Further the details of circuit equations and transformation is described in Section 3.1. (Gao, 2019)

$$P = u_{load,d}\, i_d \; + \; u_{load,q}\, i_q = u_{load,d}\, i_d$$

$$Q = u_{load,q}\, i_d \; - \; u_{load,d}\, i_q = -u_{load,d}\, i_q \tag{2.2}$$

where.

$u_{load,d}$, $u_{load,q}$: voltage along d - axis and q - axis respectively

i_d , i_q : current along d - axis and q - axis respectively

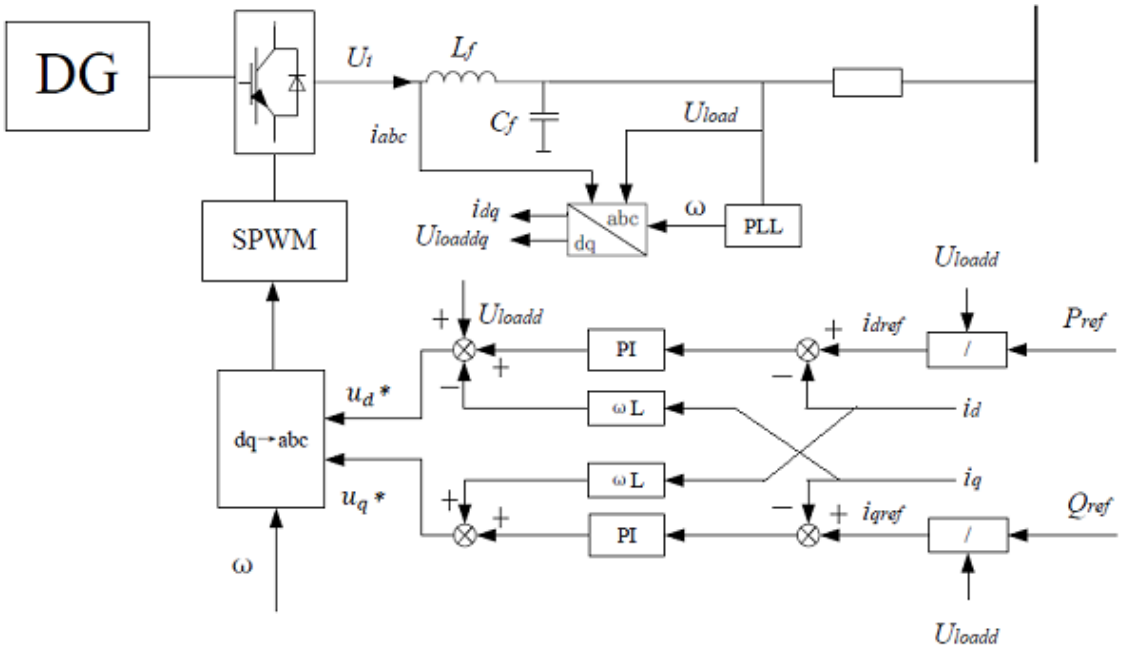

Fig. 2.4: P-Q Controller for Grid-Connected Operation of Microgrid

From equation 2.2 the reference currents in d-q frame can be evaluated which is then implemented for current loop. These currents generate the reference voltages for pulse

width modulation and hence the gate control is achieved. The typical control structure can be shown by Figure 2.4. The reference voltages is derived using KVL and Park transformation,

$u_d{}^* = u_{load,d} + R\, i_d + L\frac{d\, i_d}{dt} - \omega\, L\, i_q$

$$u_q{}^* = R\, i_q + L\frac{d\, i_q}{dt} + \omega\, L\, i_d \tag{2.3}$$

where,

$u_d{}^*$, $u_q{}^*$: reference voltage along d - axis and q - axis respectively

$u_{load,d}$: sensed load voltage converted into d-axis synchronous reference frame

R , L : Resistance and Inductance respectively

ω : frequency in rad/s

2.4 DROOP CONTROL TECHNIQUE

The characteristics of this method is similar to that of traditional generator unit which assign each DG's output power according to each DG's capability to accommodate the change in load. In this method the active power is controlled by angle which is function of frequency and the reactive power is controlled by the voltage. Equation 2.4 can be used to study the drooping characteristics which is shown in Figure 2.6. Also Figure 2.5 shows the schematic of basic droop control technique however this method is used only when system is operated in Islanded mode. (Gao, 2019)

P / f and Q / V droop characteristics,

$f = f_n - m(P - P_n)$

$$U = U_o - nQ \tag{2.4}$$

where,

f_n : rated frequency

P_n : active power at f_n

U_o : voltage at zero reactive power

m : active power droop coefficient

n : reactive power droop coefficient

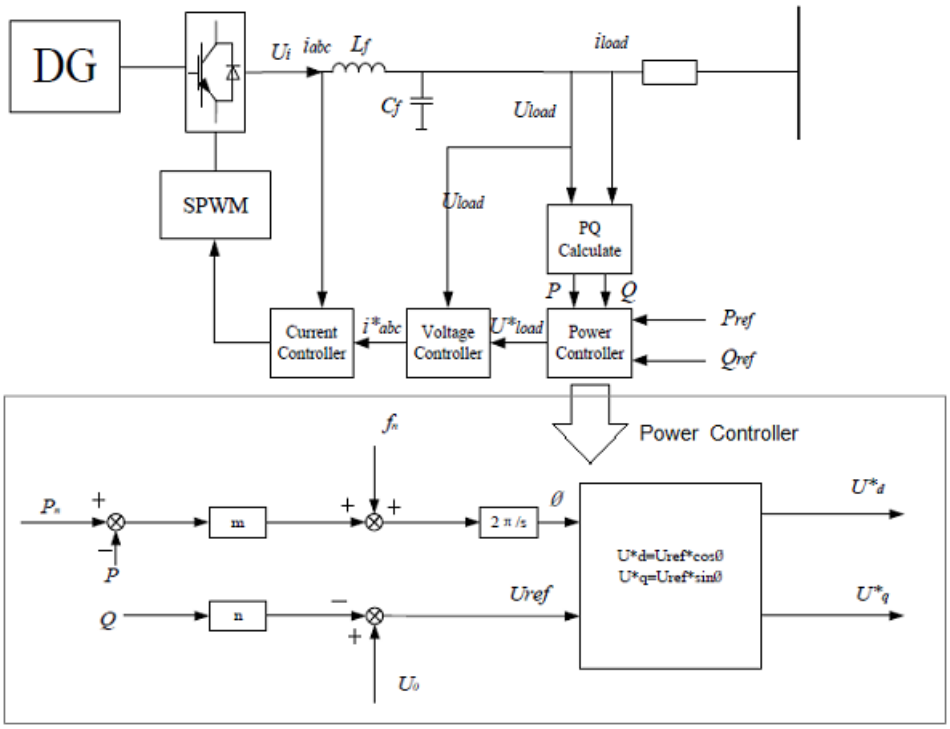

Fig. 2.5: Droop Controller

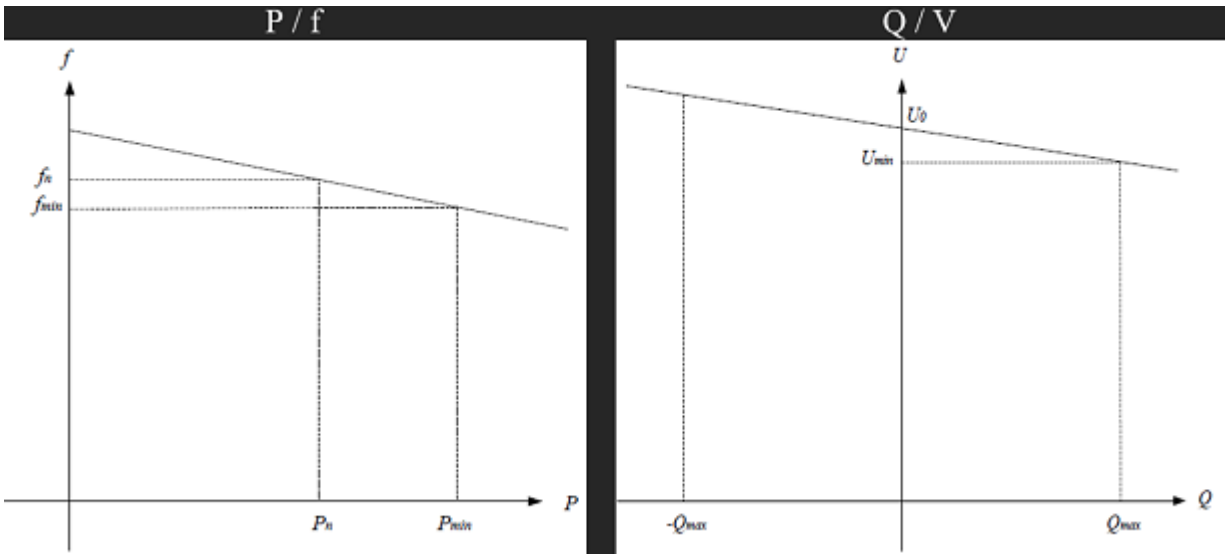

Fig. 2.6: Droop Curves

CHAPTER 3

VOLTAGE SOURCE CONVERTER

Power electronics converter in electrical system play an important role for power processing and control systems. Several converters are available out of which the voltage source converter is one of the most important component of microgrid system. Voltage Source Converter acts as interlink in between DC side of the microgrid to the AC side of the grid. (Keyhani and Marwali, 2011)

The voltage source converter can operate in

a Current Control Mode $(Grid\ Connected\ Mode)$

b Voltage Control Mode $(Off - gird\ Mode)$

According to the mode of operation the system is modelled and the control strategies are implemented as discussed in Chapter 2.

3.1 VOLTAGE SOURCE CONVERTER IN GRID CONNECTED OPERATION

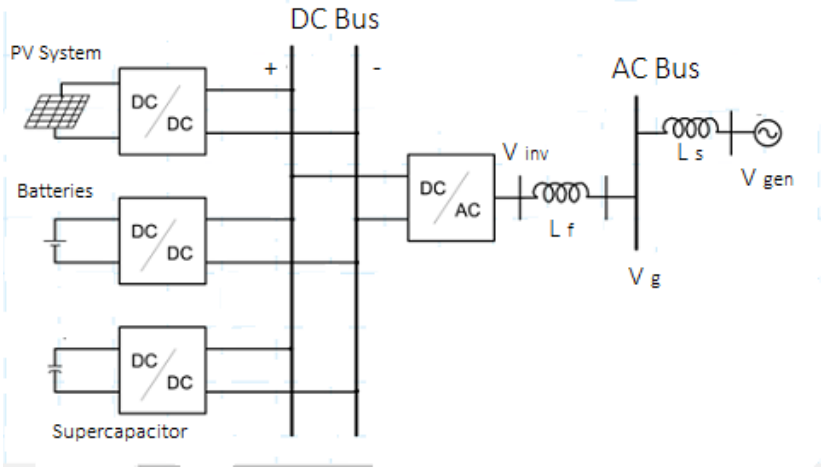

Fig. 3.1: DC Side and AC Side of Microgrid

In grid connected mode the voltage source inverter operates in current controlled mode where the controller assures appropriate power flow between the DGs (distributed generators) and the grid.

The advantages of operating voltage source converter in current controlled mode are

i Real power sharing with utility in proportion to available power at the dc link in grid interactive mode.

ii Load balancing.

iii Reactive power support.

iv Current harmonics compensation.

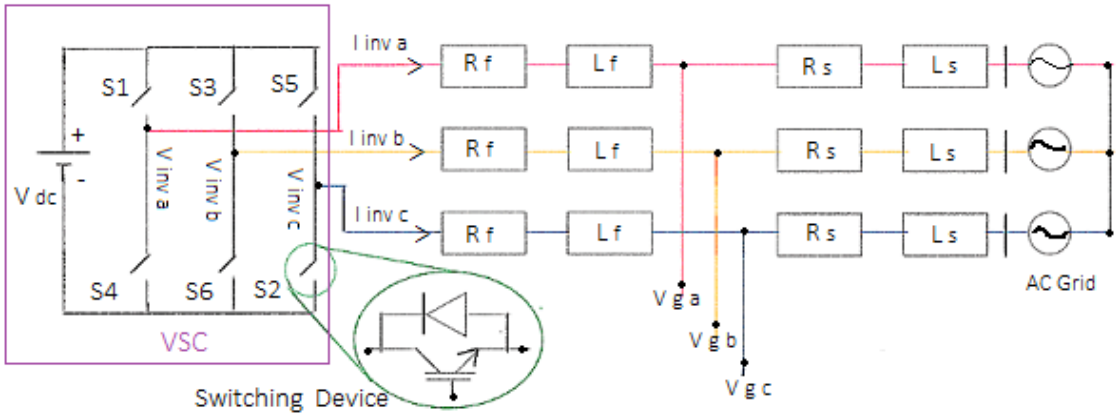

Fig. 3.2: Grid Connected VSC Model

The model has been using three phase network which consist of 3-leg converter having 6 switches ($S_1, S_2, S_3, S_4, S_5, S_6$) with DC ($V_{dc}$) voltage as input and three phase output voltage ($v_{inv,a}, v_{inv,b}, v_{inv,c}$). The three phase output voltage ($abc - frame$) can be further simplified using $d - q$ transformation where the three phase signals can be reduced into two phase signals and it is given as,

$$\begin{bmatrix} v_d \\ v_q \\ v_0 \end{bmatrix} = \sqrt{\frac{2}{3}} \begin{bmatrix} sin(\theta) & sin(\theta - 120) & sin(\theta + 120) \\ cos(\theta) & cos(\theta - 120) & cos(\theta + 120) \\ \sqrt{\frac{1}{2}} & \sqrt{\frac{1}{2}} & \sqrt{\frac{1}{2}} \end{bmatrix} \begin{bmatrix} v_a \\ v_b \\ v_c \end{bmatrix} \tag{3.1}$$

similarly, for currents,

$$\begin{bmatrix} i_d \\ i_q \\ i_0 \end{bmatrix} = \sqrt{\frac{2}{3}} \begin{bmatrix} sin(\theta) & sin(\theta - 120) & sin(\theta + 120) \\ cos(\theta) & cos(\theta - 120) & cos(\theta + 120) \\ \sqrt{\frac{1}{2}} & \sqrt{\frac{1}{2}} & \sqrt{\frac{1}{2}} \end{bmatrix} \begin{bmatrix} i_a \\ i_b \\ i_c \end{bmatrix} \tag{3.2}$$

from equation 3.1, normally $v_0 = 0$

$$v_d = \sqrt{3}\, V\, cos(\omega t - \theta) \;\; and \;\; v_q = \sqrt{3}\, V\, sin(\omega t - \theta) \tag{3.3}$$

where, V : rms value of phase voltage

Table 3.1: d-q Variables

θ	v_d	v_q
ω t	$\sqrt{3}\ V$	0
ω t - $\frac{\pi}{2}$	0	$\sqrt{3}\ V$

Thus depending upon the choice of θ, v_d and v_q are seen as constant quantity, $\sqrt{3}\, V$ or 0. This makes converter control easy in $d - q$ reference frame, as a constant value in d or q represent three phase quantities in abc reference frame. (Blaabjerg, 2018)

From Figure 3.2 using KVL

$$
\begin{aligned}
v_{inv,a} &= R_f\, i_{inv,a} \;+\; L_f\, \tfrac{d\, i_{inv,a}}{dt} \;+ v_{g,a}\;, \\
v_{inv,b} &= R_f\, i_{inv,b} \;+\; L_f\, \tfrac{d\, i_{inv,b}}{dt} \;+ v_{g,b}\;, \\
v_{inv,c} &= R_f\, i_{inv,c} \;+\; L_f\, \tfrac{d\, i_{inv,c}}{dt} \;+ v_{g,c}\;, \\
[\, v_{inv,abc}\,] &= R_f\, [\, i_{inv,abc}\,] \;+\; L_f\, \tfrac{d}{dt}[\, i_{inv,abc}\,] \;+\; [\, v_{g,abc}\,]
\end{aligned}
\tag{3.4}
$$

$$
\begin{aligned}
[\, T_{dq0}\,]^{-1}\, [\, v_{inv,dq0}\,] = R_f\, [\, T_{dq0}\,]^{-1}\, [\, i_{inv,dq0}\,] \;+\; L_f\, [\, T_{dq0}\,]^{-1}\, \tfrac{d}{dt}[\, i_{inv,dq0}\,] \\
+\, [\, T_{dq0}\,]^{-1}\, [\, v_{g,dq0}\,] \;+\; [\, \omega\, L_f\, i\,]
\end{aligned}
\tag{3.5}
$$

where,

R_f : resistance (including filter and transmission line)

L_f: inductance (including filter and transmission line)

$$
[\, v_{inv,abc}\,] = \begin{bmatrix} v_{inv,a} \\ v_{inv,b} \\ v_{inv,c} \end{bmatrix} \;;\; [\, i_{inv,abc}\,] = \begin{bmatrix} i_{inv,a} \\ i_{inv,b} \\ i_{inv,c} \end{bmatrix} \;;\; [\, v_{g,abc}\,] = \begin{bmatrix} v_{g,a} \\ v_{g,b} \\ v_{g,c} \end{bmatrix}
$$

$$
[\, v_{inv,dq0}\,] = \begin{bmatrix} v_{inv,d} \\ v_{inv,q} \\ v_{inv,0} \end{bmatrix} \;;\; [\, i_{inv,dq0}\,] = \begin{bmatrix} i_{inv,d} \\ i_{inv,q} \\ i_{inv,0} \end{bmatrix} \;;\; [\, v_{g,dq0}\,] = \begin{bmatrix} v_{g,d} \\ v_{g,q} \\ v_{g,0} \end{bmatrix}
$$

$$
[\, T_{dq0}\,]^{-1} = [\, T_{dq0}\,] = \begin{bmatrix} sin(\theta) & sin(\theta - 120) & sin(\theta + 120) \\ cos(\theta) & cos(\theta - 120) & cos(\theta + 120) \\ \sqrt{\tfrac{1}{2}} & \sqrt{\tfrac{1}{2}} & \sqrt{\tfrac{1}{2}} \end{bmatrix}
$$

$$[\,\omega\ L_f\ i\,] = \begin{bmatrix} -\,\omega\ L_f\ i_{inv,q} \\ \omega\ L_f\ i_{inv,d} \\ 0 \end{bmatrix}$$

From equation 3.4 and 3.5

$$\begin{aligned} v_{inv,d} &= R_f\ i_{inv,d}\ +\ L_f\ \tfrac{d\ i_{inv,d}}{dt}\ +v_{g,d}\ -\ \omega\ L_f\ i_{inv,q}\ , \\ v_{inv,q} &= R_f\ i_{inv,q}\ +\ L_f\ \tfrac{d\ i_{inv,q}}{dt}\ +v_{g,q}\ +\ \omega\ L_f\ i_{inv,d}\ , \\ v_{inv,0} &= R_f\ i_{inv,0}\ +\ L_f\ \tfrac{d\ i_{inv,0}}{dt}\ +v_{g,0} \end{aligned} \tag{3.6}$$

$$\begin{aligned} \Delta\ v_{i,d} &= v_{inv,d}\ -\ v_{g,d}\ , \\ \Delta\ v_{i,q} &= v_{inv,q}\ -\ v_{g,q}\ , \\ \Delta\ v_{i,0} &= v_{inv,0}\ -\ v_{g,0}\ , \\ i_{i,d} &= i_{inv,d}\ \ and\ \ i_{i,q} = i_{inv,q} \end{aligned} \tag{3.7}$$

thus, the differential equation

$$\begin{aligned} \tfrac{d\ i_{i,d}}{dt} &= \tfrac{(\ \Delta\ v_{i,d}\ -\ R_f\ i_{i,d}\ )}{L_f}\ +\ \omega\ i_{i,q}\ , \\ \tfrac{d\ i_{i,q}}{dt} &= \tfrac{(\ \Delta\ v_{i,q}\ -\ R_f\ i_{i,q}\ )}{L_f}\ -\ \omega\ i_{i,d}\ , \\ \tfrac{d\ i_{i,0}}{dt} &= \tfrac{(\ \Delta\ v_{i,0}\ -\ R_f\ i_{i,0}\ )}{L_f} \end{aligned} \tag{3.8}$$

The above equations are transformed to $s\ -\ domain$ as frequency response characteristics give guidelines to design the parameters of the system considering initial conditions to be 'zero'.

Using equation 3.6, we get

$$\begin{aligned} I_{i,d}(s) &= \tfrac{(\ V_{inv,d}(s)\ -\ V_{g,d}(s)\ +\ \omega\ L_f\ I_{i,q}(s)\ )}{(\ s\ L_f\ +\ R_f\ )}\ , \\ I_{i,q}(s) &= \tfrac{(\ V_{inv,q}(s)\ -\ V_{g,q}(s)\ -\ \omega\ L_f\ I_{i,d}(s)\ )}{(\ s\ L_f\ +\ R_f\ )}\ , \\ I_{i,0}(s) &= \tfrac{(\ V_{inv,0}(s)\ -\ V_{g,0}(s)\ )}{(\ s\ L_f\ +\ R_f\ )} \end{aligned} \tag{3.9}$$

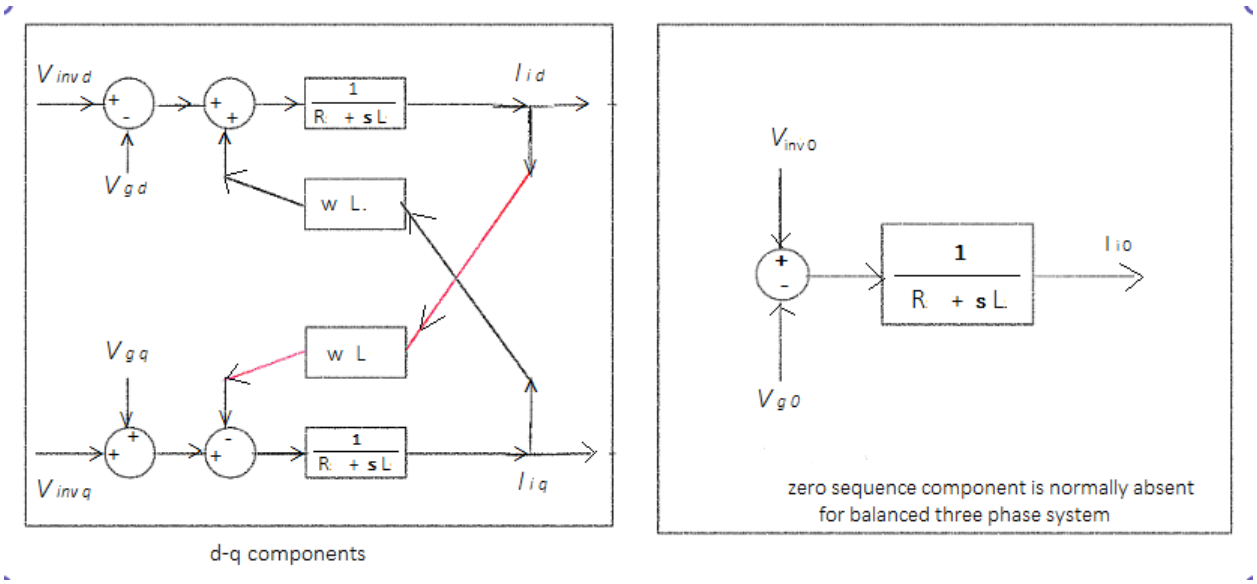

Fig. 3.3: dq0 Structural Block

3.2 SYNCHRONOUS REFERENCE FRAME PHASE LOCKED LOOP

The abc to $d-q$ transformation allows us to reduce the three phase signals into two phase signals (if '0' component neglected). From equation 3.1 and 3.2 one of the important observation has been drawn is that we can determine 'θ' by measuring ' ωt' or by locking it to a-phase voltage of grid. Thus, we can have a positive zero crossing detector to locate 'ωt = 0' and then increasing it linearly to '2π'. But, this may be difficult in case of harmonics or ripples in voltage waveform. Hence a q-axis controller can be used to determine 'θ' as,

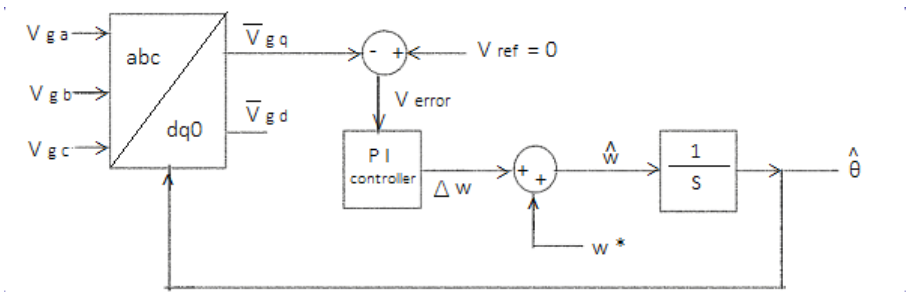

Fig. 3.4: Synchronous Reference Frame PLL

From equation 3.2,

$v_d = \sqrt{3}\,V\ cos(\,\omega t - \theta\,)$ and $v_q = \sqrt{3}\,V\ sin(\,\omega t - \theta\,)$

by setting $v_{q,ref} = V_{ref} = 0$ and comparing it with $\hat{v_q}$, the error is passed through a PI controller to generate ' $\hat{\theta}$ ' for which $\hat{v_q}$ is seen 'zero'. The estimated value of 'θ', ' $\hat{\theta}$ ' will be closely tracking ' ω t', thus $(\omega t - \hat{\theta})$ will be quite small. Hence, $sin(\omega t - \hat{\theta}) \approx (\omega t - \hat{\theta})$.

Therefore,

$$v_{q,error} = v_q - 0 \approx \sqrt{3}\, V (\omega t - \hat{\theta}) \tag{3.10}$$

Table 3.2: Operation of Synchronous Reference Frame PLL

	v_q	$v_{q,error}$	$\Delta\, \omega$	$\hat{\omega}$
$\hat{\omega} < \omega$	$+ve$	$+ve$	increases	increases to reduce v_q towards '0'
$\hat{\omega} > \omega$	$-ve$	$-ve$	decreases	decreases to increase v_q towards '0'
$\hat{\omega} = \omega$	0	0	constant	constant

Thus, this Synchronous Reference Frame PLL control ensures that ' $\hat{\omega}$ ' is tracking ' ω ' and $\hat{\theta} = \hat{\omega} t = \omega t$. Now, once we know ' $\hat{\theta}$ ' , then we have $dq0$ quantities through $dq0$ transformation. These d $dq0$ quantities are compared with their reference values, which are obtained from the desired flow of real and reactive power between the VSC and the grid.

3.3 PQ CONTROL FOR GRID CONNECTED VSC

In general, for grid connected system the real 'P' and reactive power 'Q' are assigned as reference power to the $d-q$ controller. The real power 'P' comes from the total renewable generators and reactive power 'Q' is set to support the reactive power required by the local load at the AC grid. Thus for the given power references, '$P^{\star}$' and '$Q^{\star}$', '${i_d}^{\star}$' and '${i_q}^{\star}$' are generated using following expressions,

$$p(t) = \begin{bmatrix} v_a \\ v_b \\ v_c \end{bmatrix}^T \begin{bmatrix} i_a \\ i_b \\ i_c \end{bmatrix} = \begin{bmatrix} v_d \\ v_q \\ v_0 \end{bmatrix}^T \begin{bmatrix} i_d \\ i_q \\ i_0 \end{bmatrix} \tag{3.11}$$

for three phase balanced supply, $v_0 = 0$ and $i_0 = 0$

thus,

$$p(t) = v_a\, i_a \;+\; v_b\, i_b \;+\; v_c\, i_c \;=\; v_d\, i_d \;+\; v_q\, i_q \tag{3.12}$$

Similarly, reactive power

$$q(t) = v_d\, i_q \;-\; v_q\, i_d \tag{3.13}$$

In equation 3.12 and 3.13, if we choose $\theta = \omega t$ as discussed in Synchronous Reference Frame PLL design, ' v_q' becomes 'zero' and hence the reference currents can be obtained as,

$${i_d}^{\star} = \frac{P^{\star}}{v_d} \;\; and \;\; {i_q}^{\star} = \frac{Q^{\star}}{v_d} \tag{3.14}$$

These currents are given to d and q current controller to control the voltage source converter as to maintain ' i_d ' and ' i_q ' close to ' ${i_d}^{\star}$ ' and ' ${i_q}^{\star}$ ' respectively and their three phase equivalents.

3.3.1 Closed Loop Control

from equation 3.6 and 3.7,

$$v_{inv,d} = R_f\, i_{i,d} \;+\; L_f\, \tfrac{d\, i_{i,d}}{dt} \;+ v_{g,d} \;-\; \omega\, L_f\, i_{i,q} \;,$$
$$v_{inv,q} = R_f\, i_{i,q} \;+\; L_f\, \tfrac{d\, i_{i,q}}{dt} \;+ v_{g,q} \;+\; \omega\, L_f\, i_{inv,d} \;,$$
$$v_{inv,0} = R_f\, i_{i,0} \;+\; L_f\, \tfrac{d\, i_{i,0}}{dt} \;+ v_{g,0}$$

let,

$$\begin{aligned} u_{i,d} &= R_f\, i_{i,d} \;+\; L_f\, \tfrac{d\, i_{i,d}}{dt} \;, \\ u_{i,q} &= R_f\, i_{i,q} \;+\; L_f\, \tfrac{d\, i_{i,q}}{dt} \;, \\ u_{i,0} &= R_f\, i_{i,0} \;+\; L_f\, \tfrac{d\, i_{i,0}}{dt} \end{aligned} \tag{3.15}$$

In above equations, $(\; u_{i,d}\;,\; u_{i,q}\; and\; u_{i,0}\;)$ are new control inputs. These equations shows the decoupling nature of d-q quantities as d-axis quantities depends upon only on d-components only. Same is true for q-axis. It is like to have a plant with inputs $(\; u_{i,d}\;,\; u_{i,q}\; and\; u_{i,0}\;)$ and outputs as $(\; i_{i,d}\;,\; i_{i,q}\; and\; i_{i,0}\;)$

then,

$$\begin{aligned} v_{i,d} &= u_{i,d} \;+\; v_{g,d} \;+\; \omega\, L_f\, i_{i,q} \;, \\ v_{i,q} &= u_{i,q} \;+\; v_{g,q} \;-\; \omega\, L_f\, i_{i,d} \;, \\ v_{i,0} &= u_{i,0} \;+\; v_{g,0} \end{aligned} \tag{3.16}$$

where, $(\; v_{i,d}\;,\; v_{i,q}\; and\; v_{i,0}\;)$ are actual converter output voltages. These are related to the modulating signal $(\; m_d\;,\; m_q\; and\; m_0\;)$ in $dq0$ -reference frame.

$$\begin{aligned} v_{i,d} &= \tfrac{1}{\frac{V_{dc}}{2}}\, m_d \;, \\ v_{i,q} &= \tfrac{1}{\frac{V_{dc}}{2}}\, m_q \;, \\ v_{i,0} &= \tfrac{1}{\frac{V_{dc}}{2}}\, m_0 \end{aligned} \tag{3.17}$$

and

$$
\begin{aligned}
m_d &= \frac{1}{\frac{V_{dc}}{2}} \left[u_{i,d} + v_{g,d} + \omega L_f i_{i,q} \right], \\
m_q &= \frac{1}{\frac{V_{dc}}{2}} \left[u_{i,q} + v_{g,q} - \omega L_f i_{i,d} \right], \\
m_0 &= \frac{1}{\frac{V_{dc}}{2}} \left[u_{i,0} + v_{g,0} \right]
\end{aligned}
\tag{3.18}
$$

3.3.2 PWM Control Scheme

The error signal generated by reference currents ($i_d^\star$, $i_q^\star$, $i_0^\star$) and actual currents (i_d , i_q , i_0) are passed through PI controller which generate the signals (u_d , u_q , u_0) . From these signals along with other feed-forward terms & grid d-q voltages (m_d , m_q , m_0) are generated.

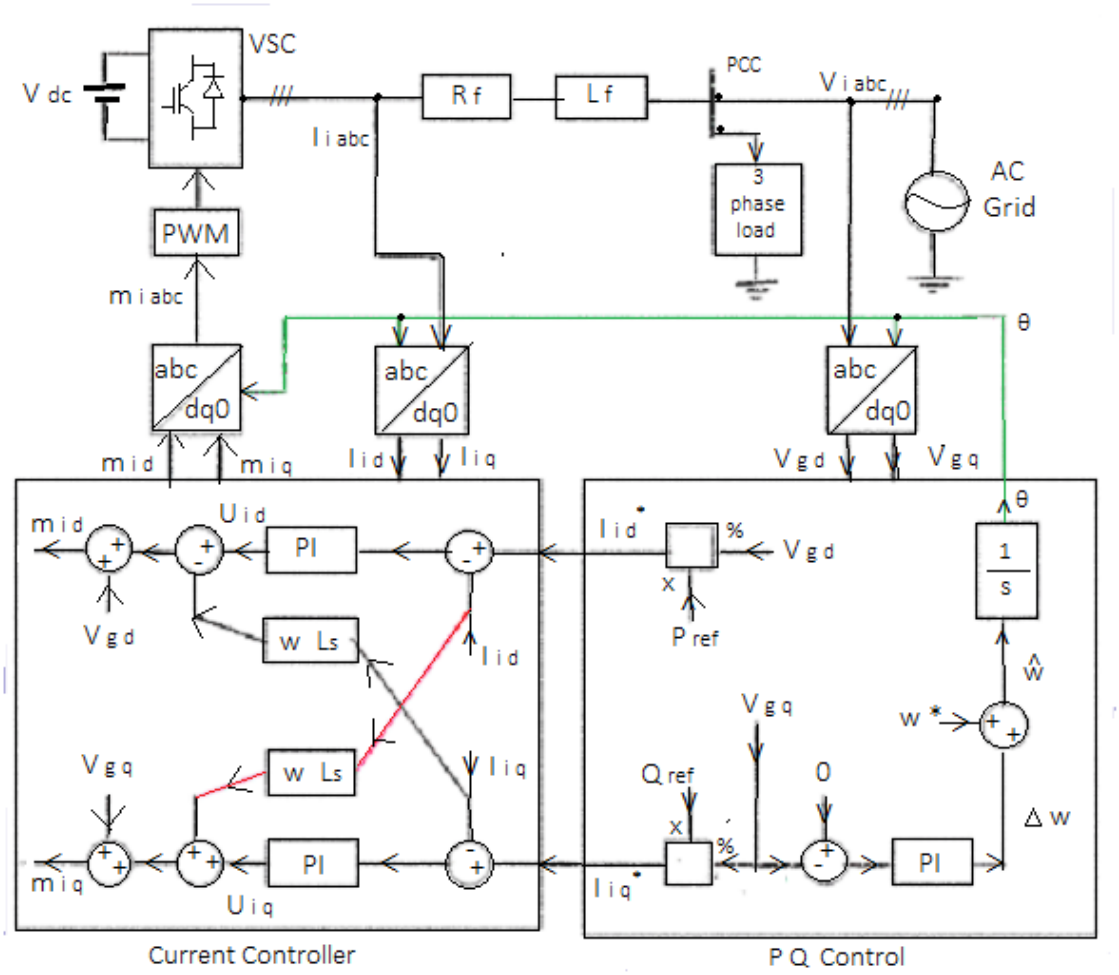

Fig. 3.5: PQ Control Technique

$$
\begin{aligned}
e_{i,d} &= i_d{}^{\star} \; - \; i_d \; \rightarrow \; u_{i,d} \; , \\
e_{i,q} &= i_q{}^{\star} \; - \; i_q \; \rightarrow \; u_{i,q} \; , \\
e_{i,0} &= i_0{}^{\star} \; - \; i_0 \; \rightarrow \; u_{i,0}
\end{aligned}
\tag{3.19}
$$

this implies,

$$
\begin{aligned}
m_d &= \tfrac{1}{\frac{V_{dc}}{2}} \left[\, u_{i,d} \; + \; v_{g,d} \; + \; \omega \, L_f \, i_{i,q} \, \right] , \\
m_q &= \tfrac{1}{\frac{V_{dc}}{2}} \left[\, u_{i,q} \; + \; v_{g,q} \; - \; \omega \, L_f \, i_{i,d} \, \right] , \\
m_0 &= \tfrac{1}{\frac{V_{dc}}{2}} \left[\, u_{i,0} \; + \; v_{g,0} \, \right]
\end{aligned}
\tag{3.20}
$$

These $(\; m_d \; , \; m_q \; , \; m_0 \;)$ are transferred back into $(\; m_a \; , \; m_b \; , \; m_c \;)$ modulating signals and PWM modulator or control unit generates switching commands to the VSC as shown in Figure 3.5

3.4 VOLTAGE SOURCE CONVERTER IN STANDALONE MODE OPERATION

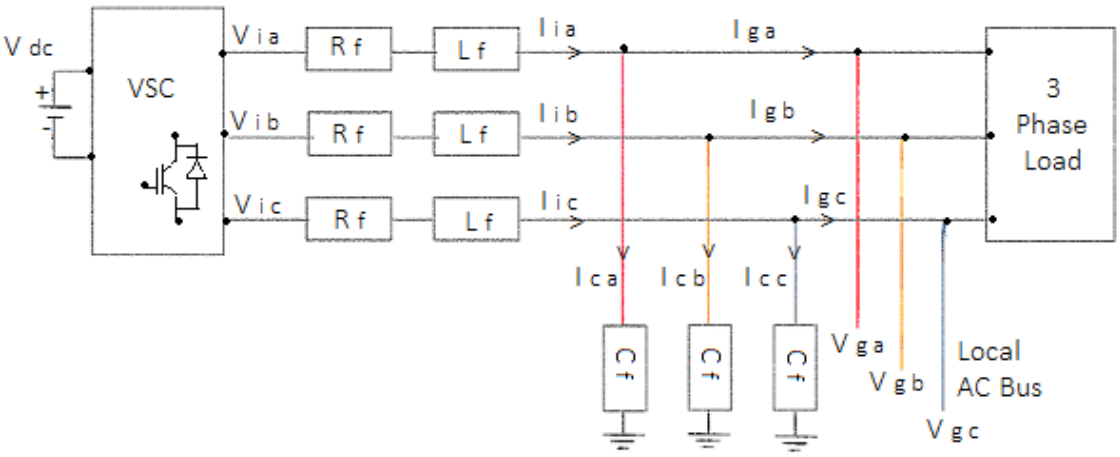

Fig. 3.6: Standalone Microgrid System

In standalone mode, the filter capacitor are used to form a local AC bus. The load currents are considered local grid currents and capacitor voltages are state variables as describe below, (Patel, 2018)

$inverter\ current = gridcurrent\ +\ capacitor\ current$

$$
\begin{aligned}
i_{inv,a} &= i_{i,a} = i_{c,a}\ +\ i_{g,a}\ , \\
i_{inv,b} &= i_{i,b} = i_{c,b}\ +\ i_{g,b}\ , \\
i_{inv,c} &= i_{i,c} = i_{c,c}\ +\ i_{g,c}
\end{aligned}
\tag{3.21}
$$

further, voltage across capacitor is nothing but grid voltage

$$
\begin{aligned}
\tfrac{d\ v_{g,a}}{dt} &= \tfrac{(\ i_{i,a}\ -\ i_{g,a}\ )}{C_f}\ , \\
\tfrac{d\ v_{g,b}}{dt} &= \tfrac{(\ i_{i,b}\ -\ i_{g,b}\ )}{C_f}\ , \\
\tfrac{d\ v_{g,c}}{dt} &= \tfrac{(\ i_{i,c}\ -\ i_{g,c}\ )}{C_f}\ ,
\end{aligned}
\tag{3.22}
$$

In Matrix form,

$$
[\ i_{i,abc}\ ] = C_f\ \frac{d}{dt}[\ v_{g,abc}\ ]\ +\ [\ i_{g,abc}\ ] \tag{3.23}
$$

After applying d-q transformation to above model, we get

$$
[\ i_{i,dq0}\ ] = C_f\ \frac{d}{dt}[\ v_{g,dq0}\ ]\ +\ [\ i_{g,dq0}\ ]\ +\ [\ \omega\ C_f\ v\ ] \tag{3.24}
$$

where, C_f : filter capacitance

$$
[\ i_{i,abc}\ ] = \begin{bmatrix} i_{i,a} \\ i_{i,b} \\ i_{i,c} \end{bmatrix}\ ;\ [\ v_{g,abc}\ ] = \begin{bmatrix} v_{g,a} \\ v_{g,b} \\ v_{g,c} \end{bmatrix}\ ;\ [\ i_{g,abc}\ ] = \begin{bmatrix} i_{g,a} \\ i_{g,b} \\ i_{g,c} \end{bmatrix}
$$

$$[\, i_{i,dq0} \,] = \begin{bmatrix} i_{i,d} \\ i_{i,q} \\ i_{i,0} \end{bmatrix} \;;\; [\, v_{g,dq0} \,] = \begin{bmatrix} v_{g,d} \\ v_{g,q} \\ v_{g,0} \end{bmatrix} \;;\; [\, i_{g,dq0} \,] = \begin{bmatrix} i_{g,d} \\ i_{g,q} \\ i_{g,0} \end{bmatrix}$$

$$[\, \omega\, C_f\, v \,] = \begin{bmatrix} -\,\omega\, C_f\, v_{g,q} \\ \omega\, C_f\, v_{g,d} \\ 0 \end{bmatrix}$$

thus, the differential equation

$$\begin{aligned} \frac{d\, v_{g,d}}{dt} &= \frac{(\, i_{i,d} - i_{g,d}\,)}{C_f} + \omega\, v_{g,q}, \\ \frac{d\, v_{g,q}}{dt} &= \frac{(\, i_{i,q} - i_{g,q}\,)}{C_f} - \omega\, v_{g,d}, \\ \frac{d\, v_{g,0}}{dt} &= \frac{(\, i_{i,0} - i_{g,0}\,)}{C_f}\,, \end{aligned} \tag{3.25}$$

Equation 3.8 & 3.25 form first order differential equations in $(\, i_{i,d}\,,\; i_{i,q}\,,\; i_{i,0}\,,\; v_{g,d}\,,\; v_{g,q}\,,\; v_{g,0}\,)$ together represent the system dynamics. Equation 3.8 involve current cross coupling terms and equation 3.25 involve voltage cross coupling terms.

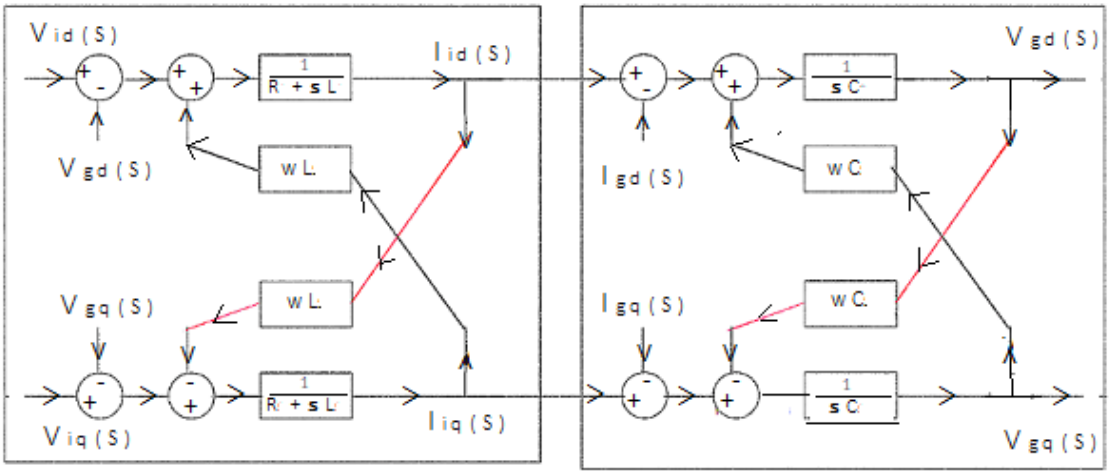

Fig. 3.7: Plant Model For Microgrid System in Standalone Mode

Transforming equation 3.8 & 3.25 to $s-domain$ as frequency response characteristics give guidelines to design the parameters of the system considering initial conditions to

be ‘zero’

Current controller loop

$$
\begin{aligned}
I_{i,d}(s) &= \frac{(\ V_{i,d}(s) - V_{g,d}(s) + \omega\ L_f\ I_{i,q}(s)\ )}{(\ s\ L_f\ +\ R_f\ )}\ , \\
I_{i,q}(s) &= \frac{(\ V_{i,q}(s) - V_{g,q}(s) - \omega\ L_f\ I_{i,d}(s)\ )}{(\ s\ L_f\ +\ R_f\ )}\ , \\
I_{i,0}(s) &= \frac{(\ V_{i,0}(s) - V_{g,0}(s)\ )}{(\ s\ L_f\ +\ R_f\ )}
\end{aligned}
\tag{3.26}
$$

Voltage controller loop

$$
\begin{aligned}
V_{g,d}(s) &= \frac{(\ I_{i,d}(s) - I_{g,d}(s) + \omega\ C_f\ V_{g,q}(s)\ )}{(\ s\ C_f\ )}\ , \\
V_{g,q}(s) &= \frac{(\ I_{i,q}(s) - I_{g,q}(s) - \omega\ C_f\ V_{g,d}(s)\ )}{(\ s\ C_f\ )}\ , \\
V_{g,0}(s) &= \frac{(\ I_{i,0}(s) - I_{g,0}(s)\ )}{(\ s\ C_f\ )}
\end{aligned}
\tag{3.27}
$$

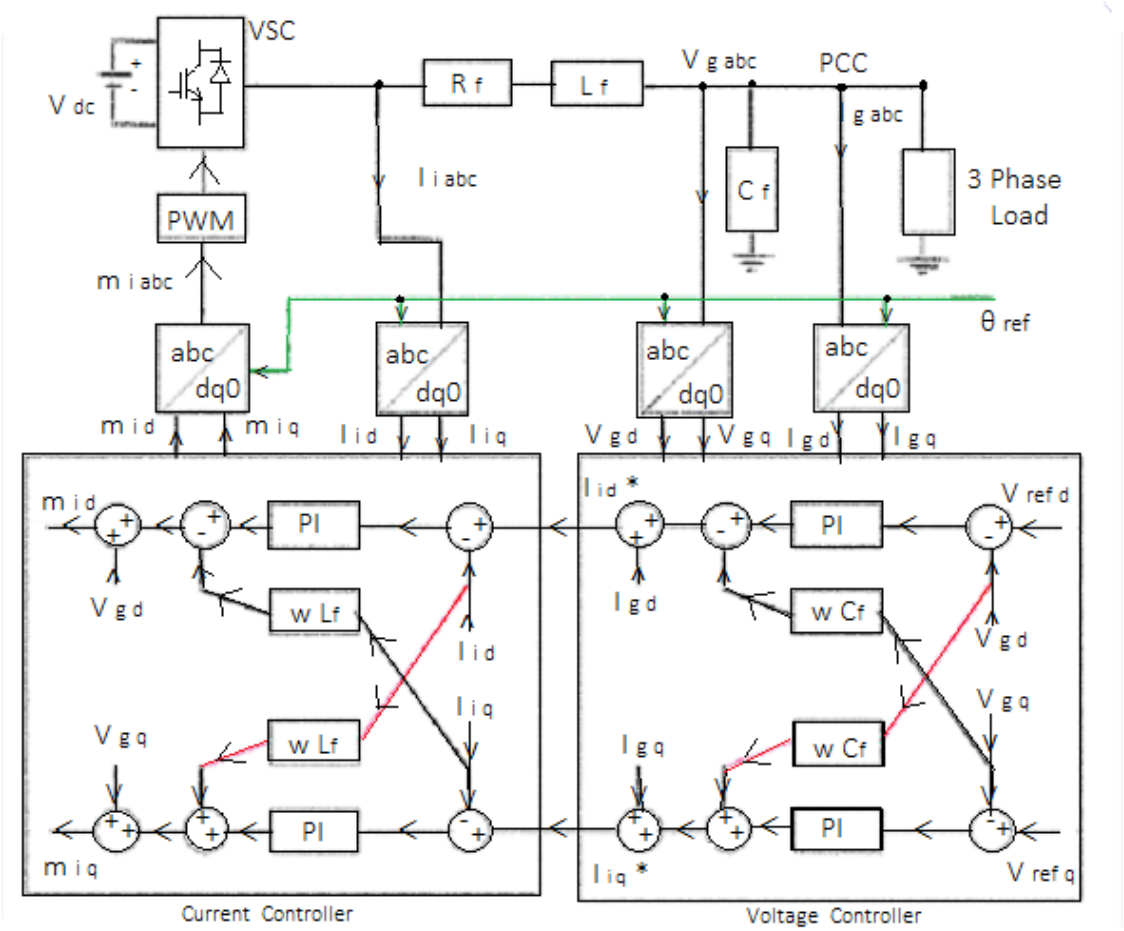

Fig. 3.8: Controller Realization for Standalone Microgrid System

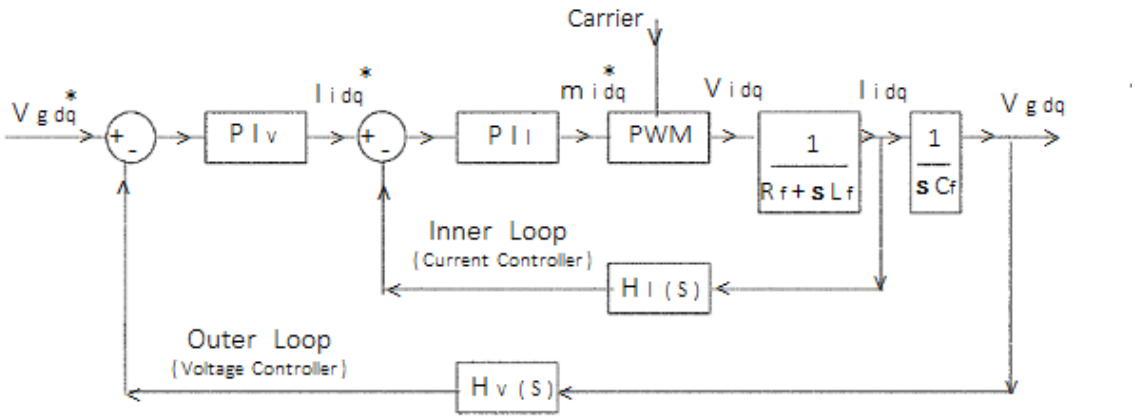

Fig. 3.9: Control Structure for Standalone Microgrid System

Design Guidelines :

i Bandwidth for inner current control loop should be $\frac{1}{10^{th}}$ of the carrier frequency

ii Bandwidth for outer voltage control loop should be $\frac{1}{10^{th}}$ of the current control loop.

CHAPTER 4

SIMULATION Grid Connected Mode

Table 4.1: System Specification for Grid Connected Mode

f_s	(kHz)	10	Switching frequency
f_c	(kHz)	1	Current controller frequency
f_p	(Hz)	100	PQ controller frequency
$Grid\ Side$	$---$	$---$	$---$
V	(V)	230	(phase voltage)
f	(Hz)	50	(nominal frequency)
$Inverter\ Side$	$---$	$---$	$---$
Vdc	(V)	800	(battery DC voltage)
Lf	(H)	0.04	(overall Inductor)
Rf	(Ω)	1	(overall Resistor)
$Load\ Side$	$---$	$---$	$---$
pf	$cos(\theta)$	0.99	(power factor)
Pref	(kW)	9	(Real Power Ref.)
Qref	$(kVAr)$	0.666	(Reactive Power Ref.)

The simulation for control of grid connected voltage source converter is simulated on MATLAB and following outputs have been observed. The PQ control technique with Synchronous Reference Frame Phase Locked Loop has been implemented for the microgrid system specified in table 4.1. Here, we have modelled the microgrid with single inverter to test the performance when load demand is of 9.025 kVA.

Current Controller Response : Figure 4.1 & Figure 4.2

PQ Controller Response : Figure 4.3 & Figure 4.4

Controllers : Figure 4.5 & Figure 4.6

Outputs : Figure 4.7 , Figure 4.8 & Figure 4.9

Load Phase Voltages and Currents : Figure 4.10

Load Voltage and THD : Figure 4.11

Load Current and THD : Figure 4.12

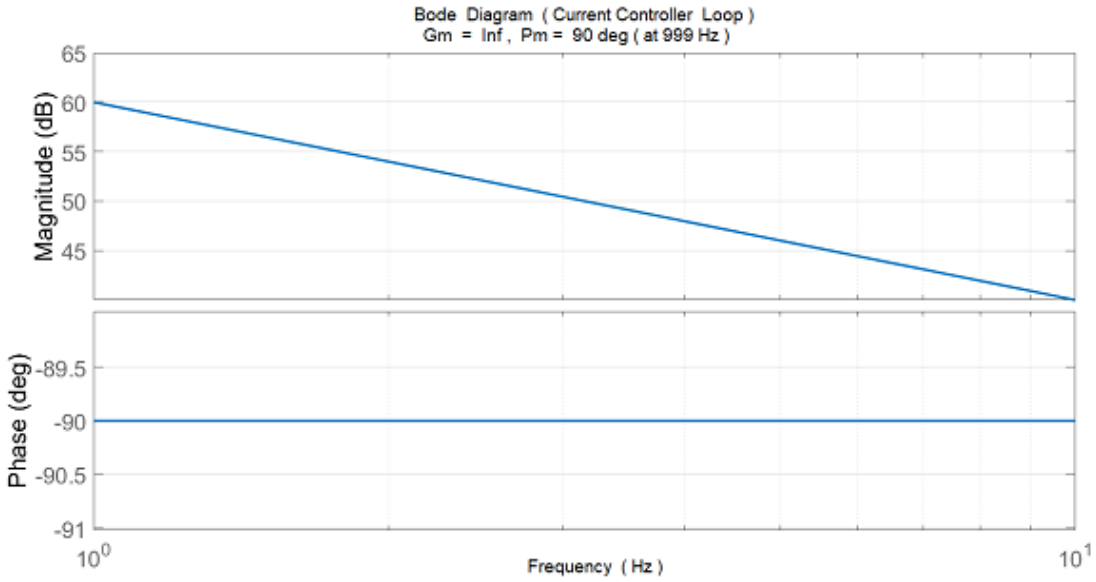

Fig. 4.1: Current Controller Frequency Response

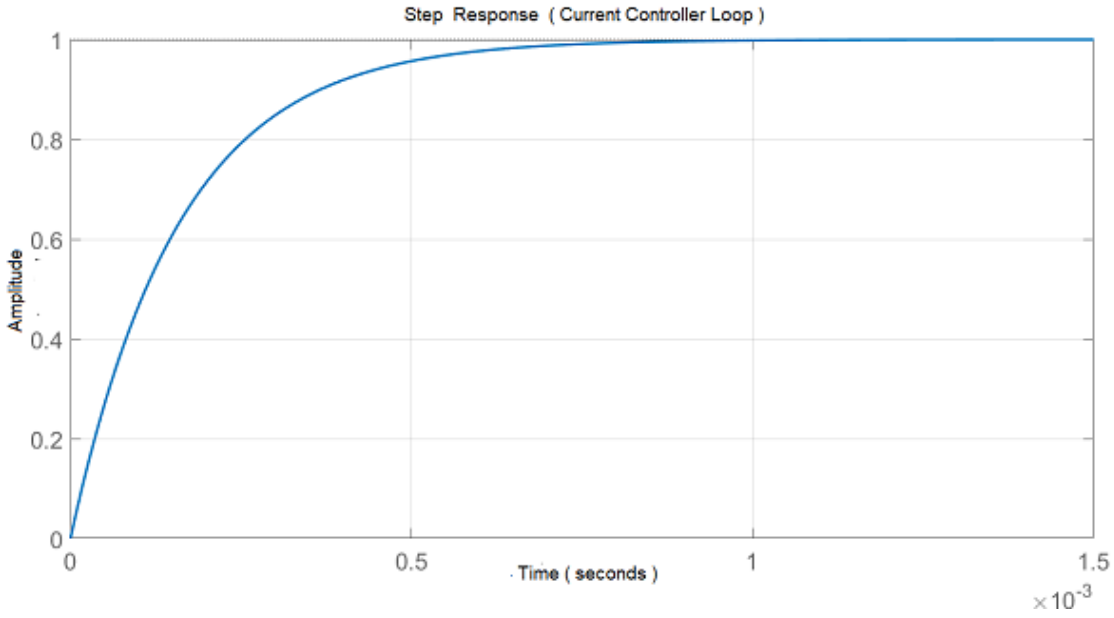

Fig. 4.2: Current Controller Unit-Step Response

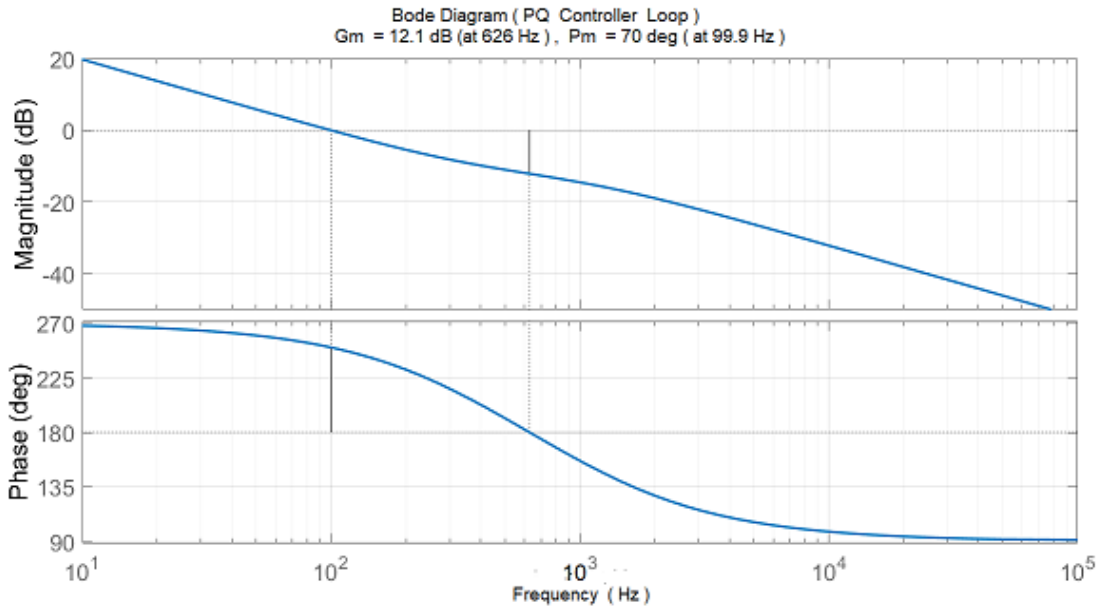

Fig. 4.3: PQ Controller Frequency Response

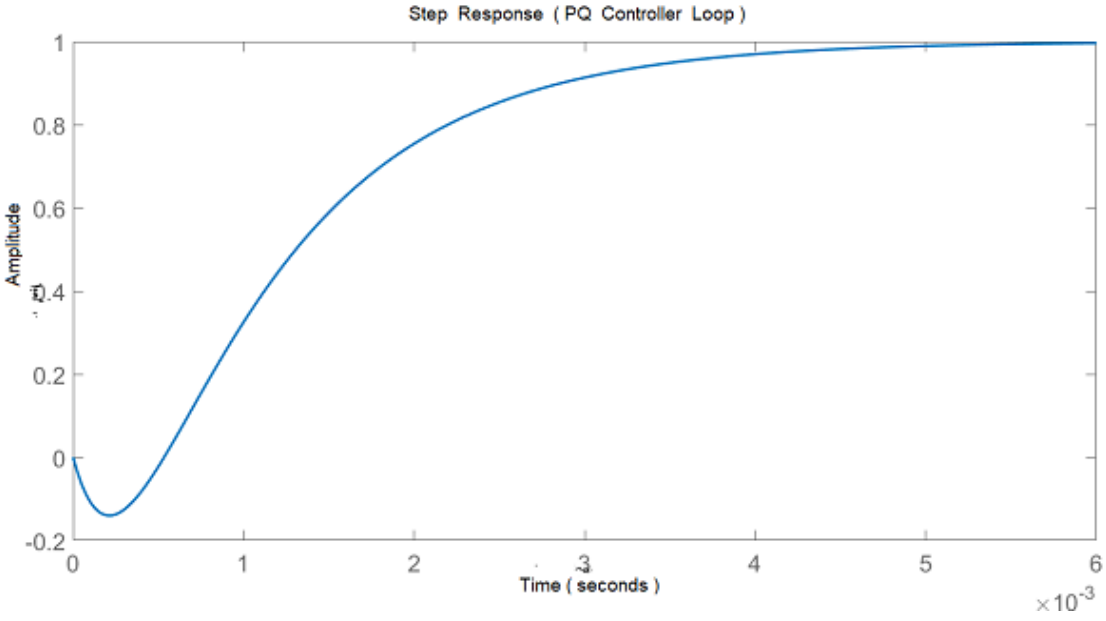

Fig. 4.4: PQ Controller Unit-Step Response

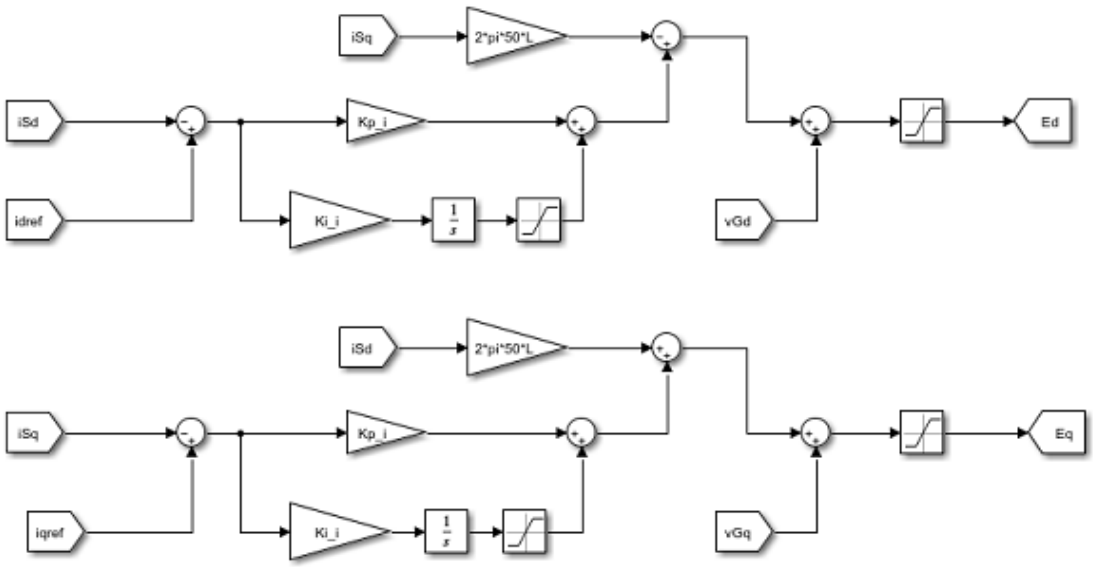

Fig. 4.5: Inner - Current Controller Loop

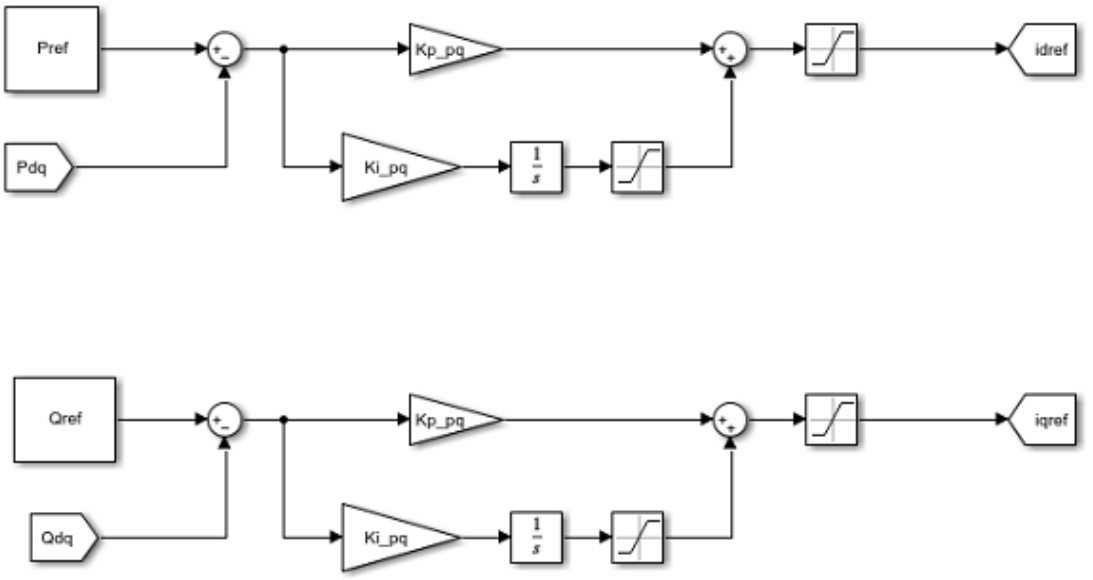

Fig. 4.6: Outer - Power Controller Loop

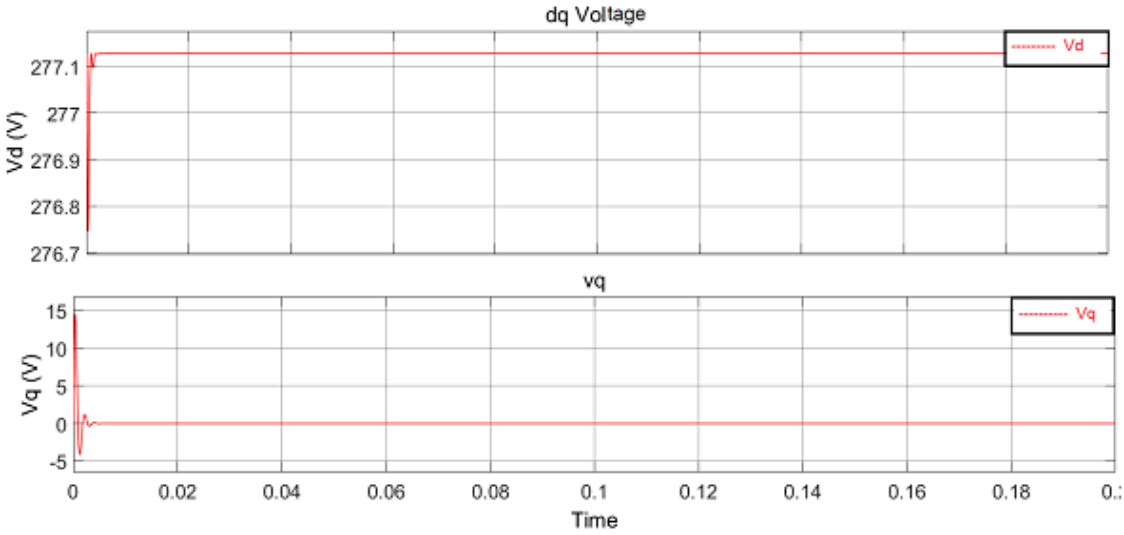

Fig. 4.7: d-q voltages

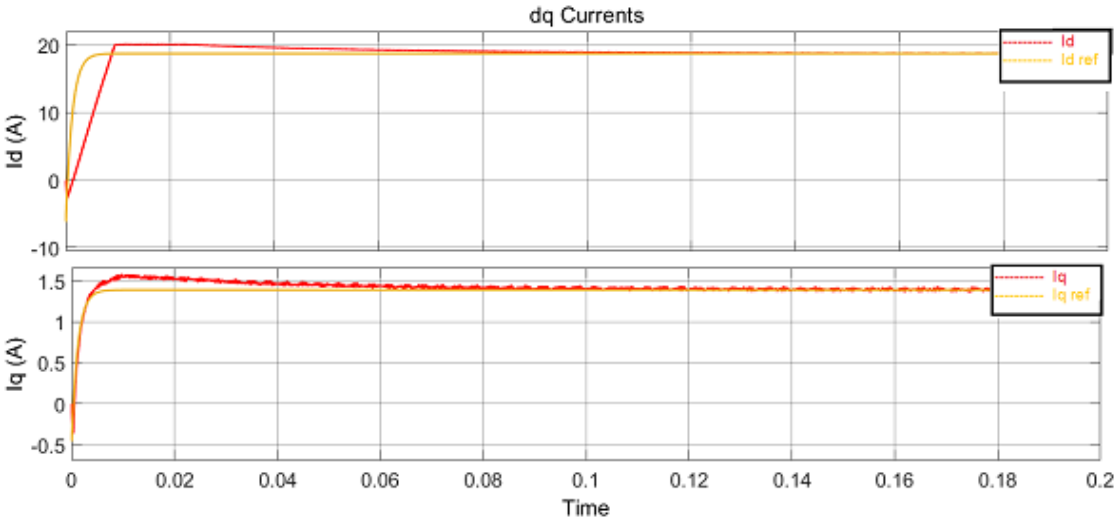

Fig. 4.8: Current Loop

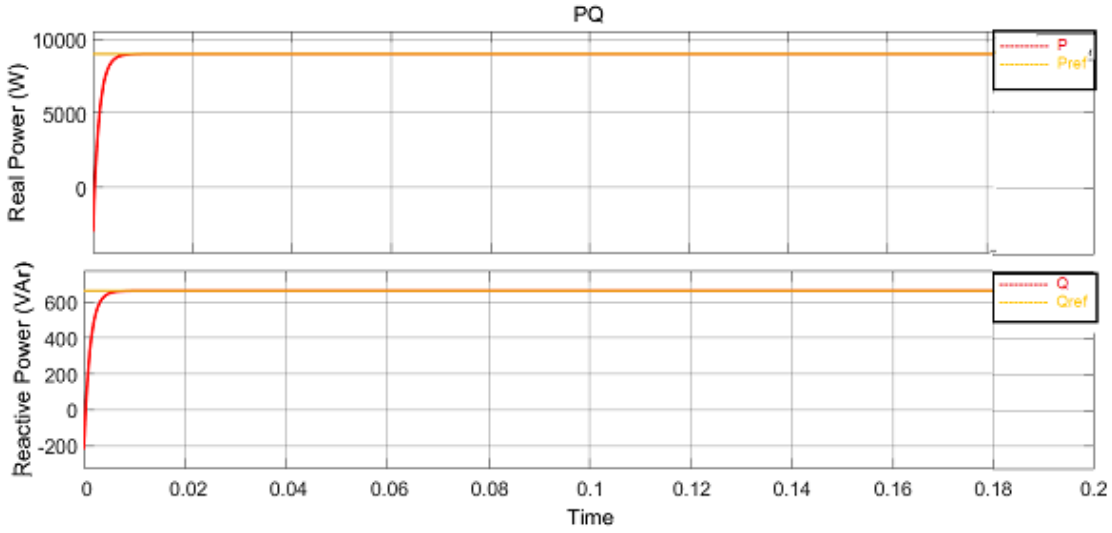

Fig. 4.9: PQ Waveforms

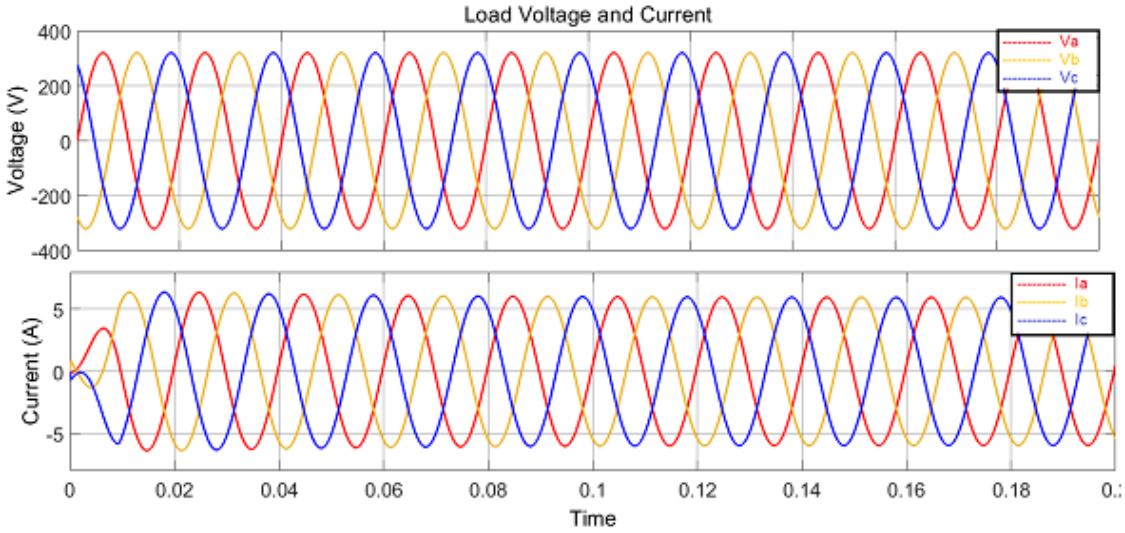

Fig. 4.10: Load Phase Voltages and Currents

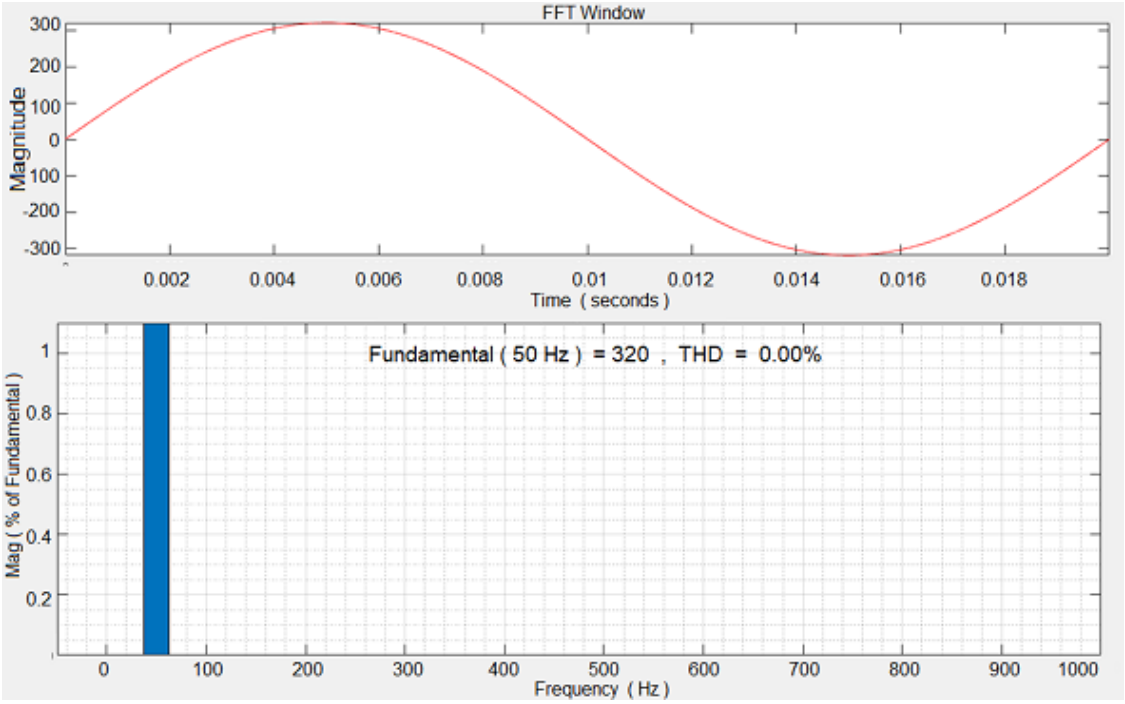

Fig. 4.11: Load Voltage and THD

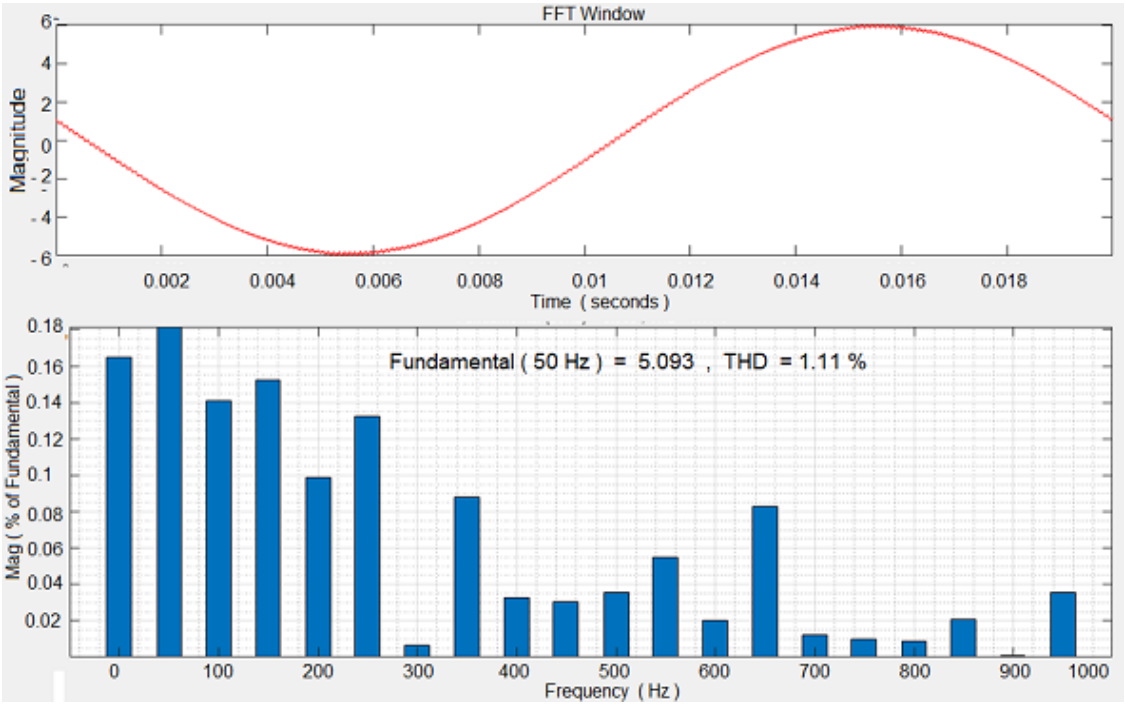

Fig. 4.12: Load Current and THD

CHAPTER 5

SIMULATION Standalone Mode

Table 5.1: System Specification for Standalone Mode

f_s	(kHz)	10	Switching frequency
f_c	(kHz)	1	Current controller frequency
f_p	(Hz)	100	Voltage controller frequency
$Load\ Side$	$---$	$---$	$---$
V	(V)	230	(phase voltage)
f	(Hz)	50	(nominal frequency)
$Inverter\ Side$	$---$	$---$	$---$
Vdc	(V)	800	(battery DC voltage)
Lf	(H)	0.1	(overall Inductor)
Rf	(Ω)	1	(overall Resistor)
Cf	(μF)	160	(overall Capacitor)
$Load\ Side$	$---$	$---$	$---$
pf	$cos(\theta)$	0.95	(power factor)
Pref	(kW)	150	(Real Power Ref.)
Qref	$(kVAr)$	50	(Reactive Power Ref.)

The simulation for control of voltage source converter in Standalone mode is simulated on MATLAB and following outputs have observed. The PQ control technique with Droop Control Technique has been implemented for the microgrid system specified in table 5.1. Here, we have modelled the microgrid with four identical inverters having same specifications as that of an inverter used in grid-connected operation in order to test the performance when load demand is of 158 kVA. The droop controller is set with parameters as P/f droop ratio = 1 % (meaning variation of 1% in operating frequency is allowed w.r.t nominal frequency) and Q/V droop ratio = 4 % (meaning a variation of 4% in operating voltage is allowed w.r.t nominal voltage)

Outputs : Figure 5.1 & Figure 5.2

Load Phase Voltages and Currents : Figure 5.3

Load Voltage and THD : Figure 5.4

Load Current and THD : Figure 5.5

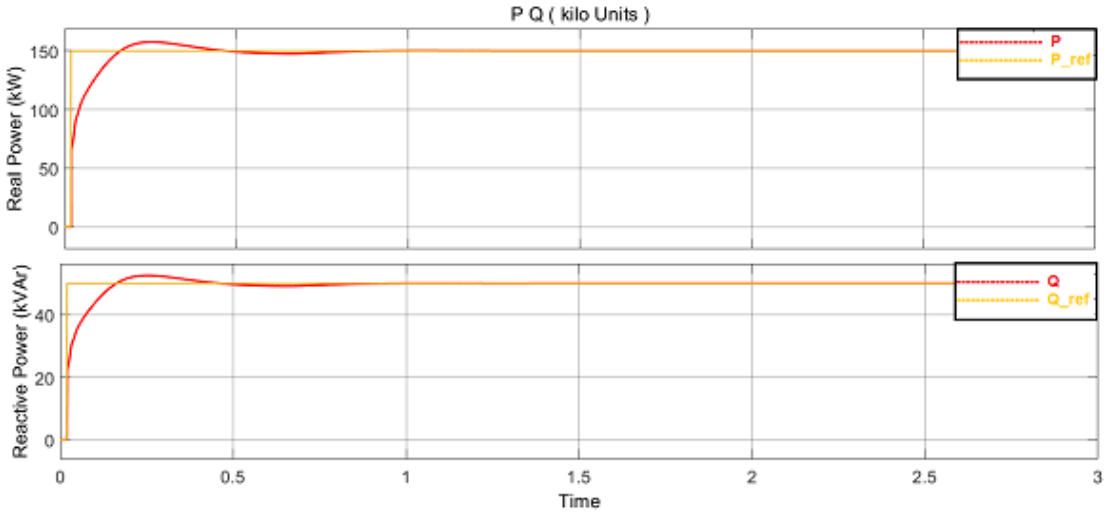

Fig. 5.1: PQ Output

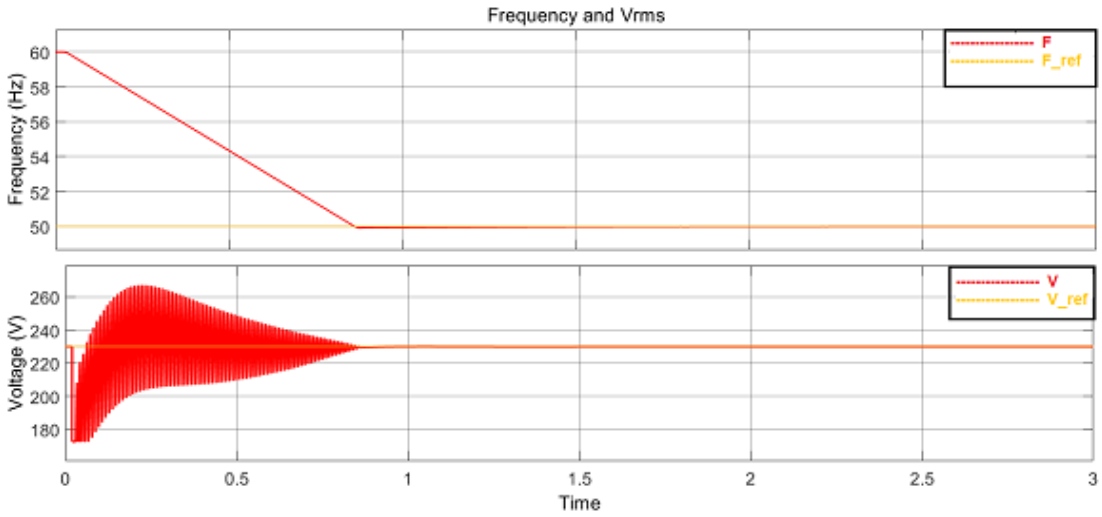

Fig. 5.2: Frequency and Voltage

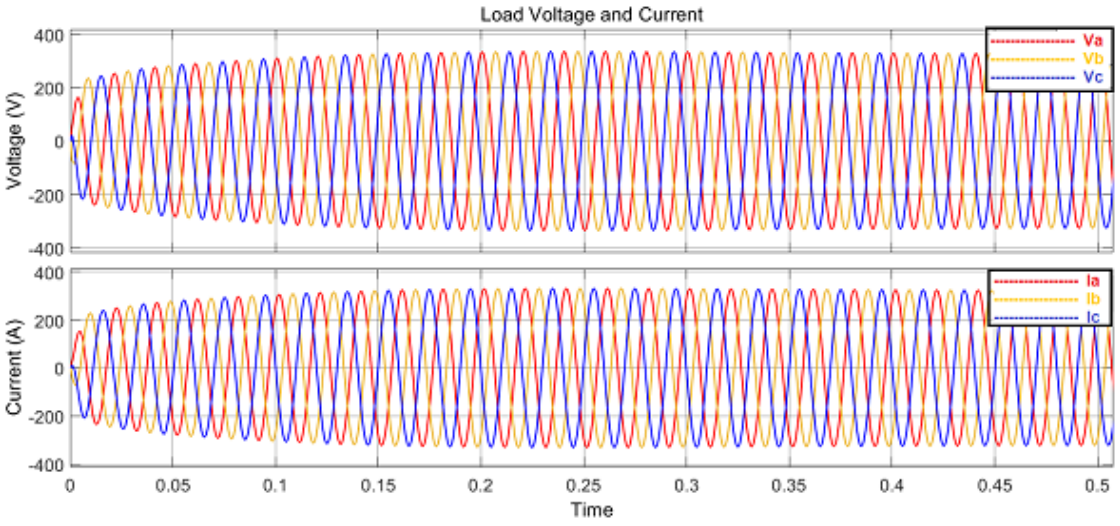

Fig. 5.3: Load Phase Voltages and Currents

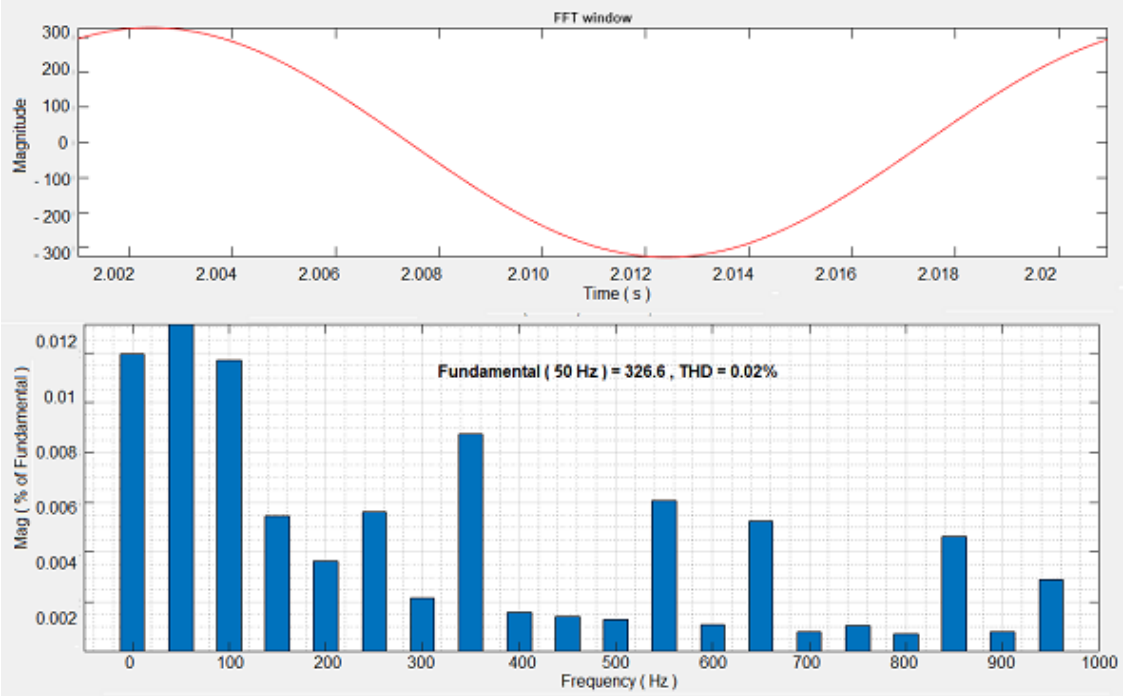

Fig. 5.4: Load Voltage and THD

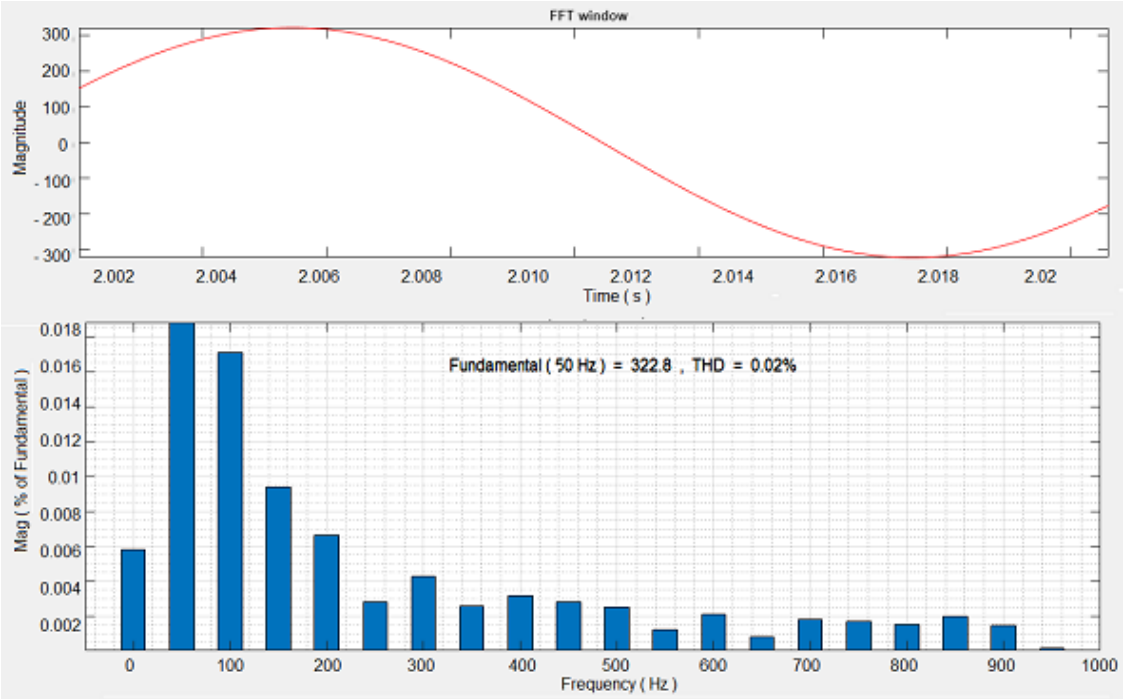

Fig. 5.5: Load Current and THD

CHAPTER 6

Results and Conclusion

6.1 RESULTS

6.1.1 Grid Connected Mode

The open loop characteristic of current controller, Figure 4.1 & Figure 4.2 has been studied and the PI controller parameters are designed and we found following results :

- The gain margin is "infinite" and phase margin is 90° (at 999 Hz).
- The current controller is achieving a steady state value within 1 ms which is desired for our current controller.

The open loop characteristic of pq controller, Figure 4.3 & Figure 4.4 has been studied and the PI controller parameters are designed and we found following results :

- The gain margin is 12.1 db (at 626 Hz) and phase margin is 70° (at 99.9 Hz).
- The pq controller is achieving a steady state value within 10 ms which is desired for our pq controller.

The simulation results, Figure 4.5 - Figure 4.12 shows the microgrid shares the required power to load connected with grid. The THD values are within limits as per IEEE standard 519-1992.

6.1.2 Standalone Mode

The simulation results, Figure 5.1 - Figure 5.5 shows the microgrid when operating in standalone mode shares the required power to load connected with local ac grid. Further, the frequency of operation (49.95 Hz < f < 50.05 Hz) and voltage level (220.8 V < $V_{rms,phase}$ < 239.2 V) are within the limits as set in droop controller. Also, the THD values don't violate the IEEE standard 519-1992.

6.2 CONCLUSION

PV and battery based renewable energy systems have wide application at both domestic and industrial level. Such systems are really helpful to form a small-scale microgrid so that it can share the electrical load within the system or with the main ac grid whenever there's excess generation of power on microgrid side. This thesis has provided some basic idea about its analysis and performance. Further, such system has great importance as the new concept of energy trading is been adopted across the world.

APPENDIX A

Energy Storage System

Energy storage system refers to the device used for converting one form of energy into a form that can be stored and can be used later based on the need or requirement in the required form of energy. Energy storage system and technology available with ESS will become increasingly important in delivering energy in near future especially when we refer to microgrid system (electric power system) which helps in power balancing and the objective of carbon-neutralizing by promoting applications of renewable energy systems. There's no doubt, it has potential to transform electric industry because without energy storage system, a 100 % renewable energy grid will not be possible. Energy storage system along with microgrid and main power grid can help to integrate renewable energy effectively and reliably, especially those with a variable output, such as solar, wind, ocean wave and tidal generation. (Ashok Jhunjhunwala, 2021)

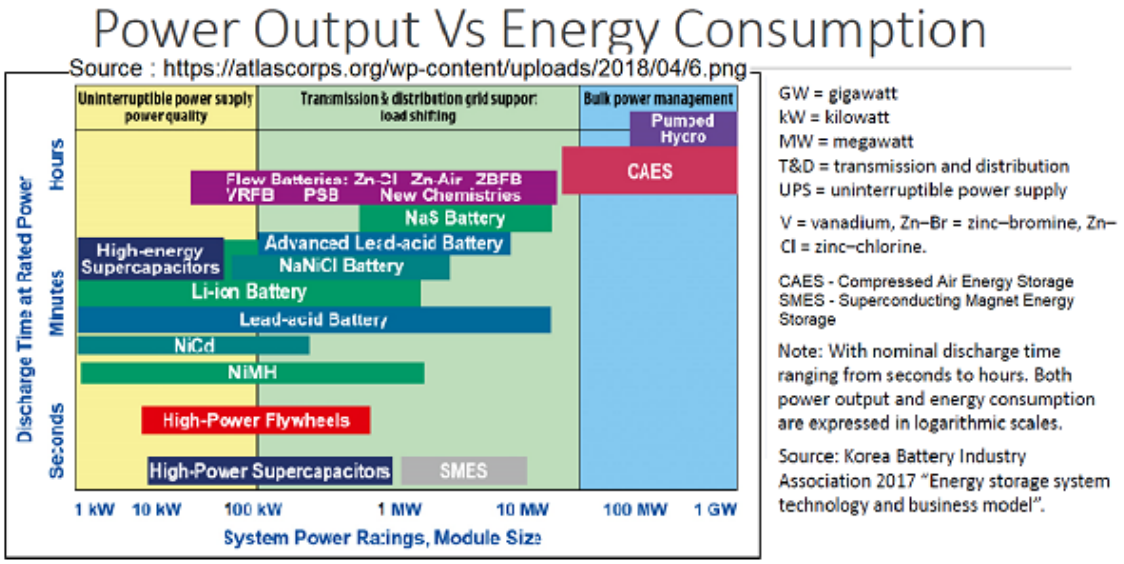

Fig. A.1: Power Output vs Energy Consumption

The integration of renewable energy however possess some additional challenges. One of the challenge is the temporal difference between generation and demand. Solar

energy generates electricity (at peak level) during afternoon but at night generation goes down. Similarly, for wind energy the evening time is favourable to generate electricity however the seasonal variation affects its performance. So, it is essential to adopt energy storage system which can be helpful to store energy during peak generation hours and later it can be used for short (for several hours during night, in case of solar energy system) or for long term duration (for several months, in case of hydro and wind energy system). The energy storage system can also be used for very short duration. Suppose in solar system, the irradiance is changing over time (seconds or minutes) creating fluctuations at output, on other hand, the wind speed is also keep changing its value every second creating fluctuations at output of wind-turbine.

Thus, following are some of the characteristics/objectives of energy storage system –

1 It increases reliability and flexibility of renewable energy generator (solar, wind, etc.)

2 It is useful in uninterrupted power supply (UPS) applications

3 Transmission and distribution system support in terms of load balancing

4 Bulk power management (for future expansion)

5 Helps in delivering right amount of power with right specifications from unanticipated power generators like solar and wind

6 Helps in supply power during peak demand and reduce the load on grid

7 Lower grid rejection loss to accommodate the projected installation of solar and wind energy in future grids

Figure A.1 gives a general idea about different storage options and their applications according to the objectives. The different types of energy storage systems are shown in the schematic shown by figure A.2.

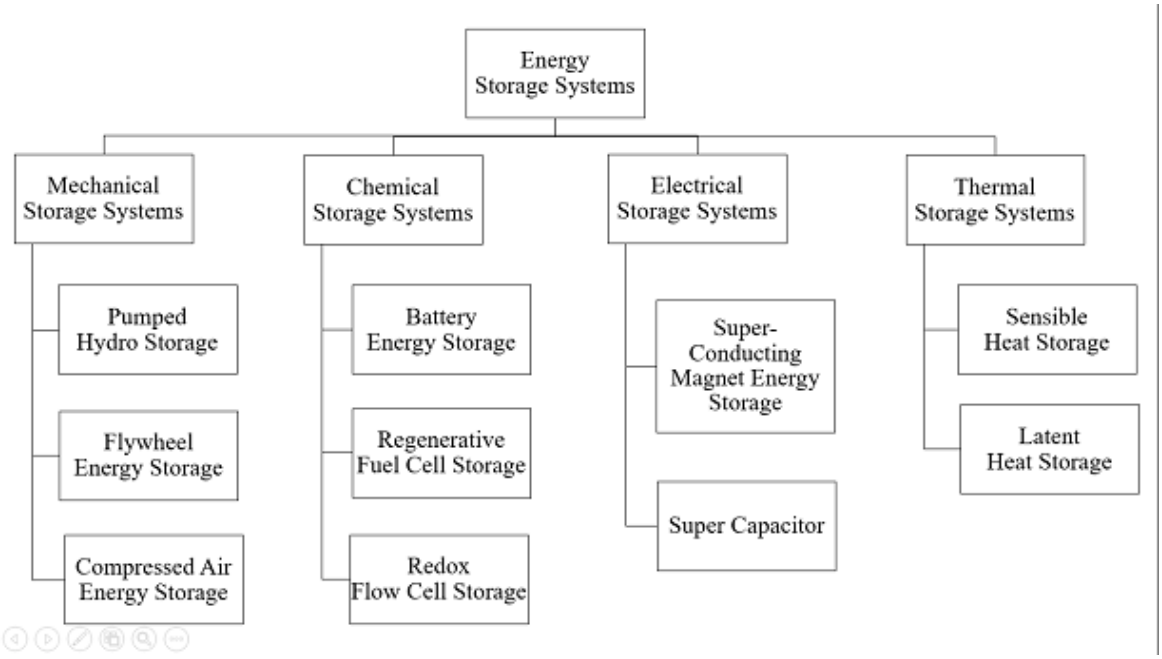

Fig. A.2: Energy Storage Systems

APPENDIX B

MOSFET vs IGBT

Table B.1: MOSFET vs IGBT Comparission

MOSFET	IGBT
• Unipolar / Majority carrier device due to which there's no conductivity modulation happens and hence no process like active recombination phenomena takes place.	• Bipolar / Minority carrier device due to which there's conductivity modulation happens and hence natural/active recombination affects the switching characteristics.
• The physical construction has inherently present diode which makes the device easy for parallel operation.	• It does not have any diode inherently present in its physical construction hence additional diode is required for freewheeling process.
• Since, due to absence of tailing current in it switching characteristics and due to above two reasons it is faster than IGBT.	• Since, along with diode recovery period, it has tailing collector current due to the stored charge in n type – drift region hence it is slower than MOSFET.
• Switching losses are lower.	• Due to tail current switching losses are high (off-state).
• MOSFET has high on-state resistance due to which it is used in low voltage applications.	• It has low on-state resistance due to which it is used in high voltage applications.

Reference (Sattar, 2016)

Table B.2: MOSFET and IGBT Power Application

Characteristics	MOSFET	IGBT
Frequency (kHz)	High (> 20)	Low (< 20)
Voltage (kV)	Low (< 0.5)	High (> 1)
Cycles	Long-duty	Low-duty

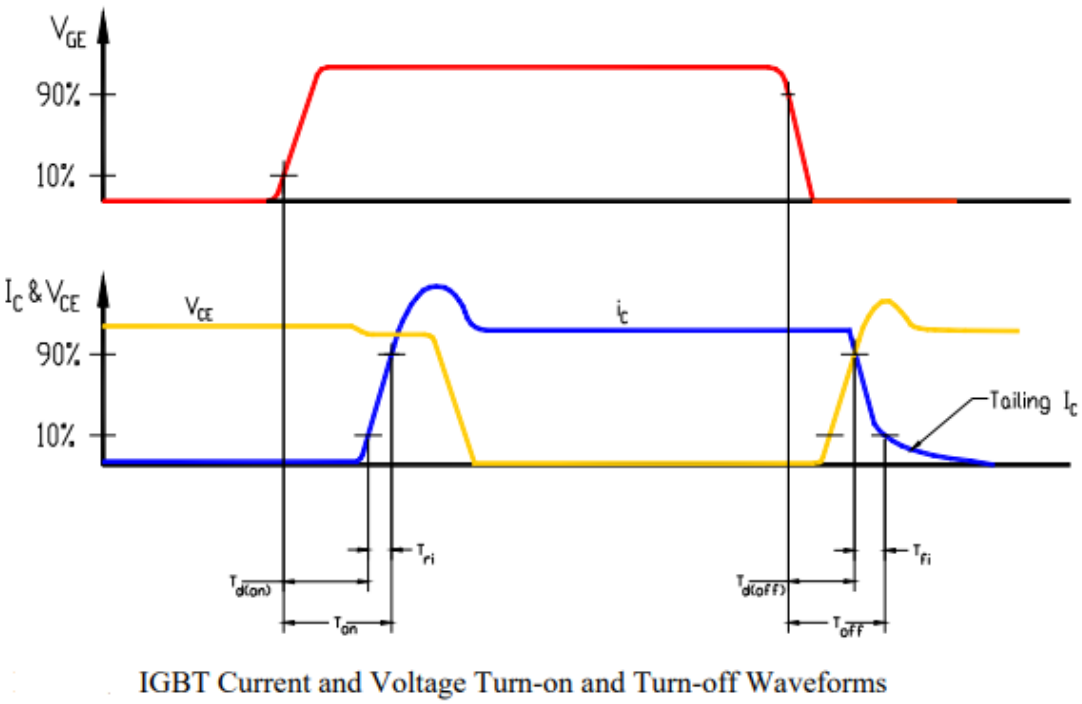

IGBT Current and Voltage Turn-on and Turn-off Waveforms

Fig. B.1: IGBT Switching Characteristic

APPENDIX C

Reference Frames

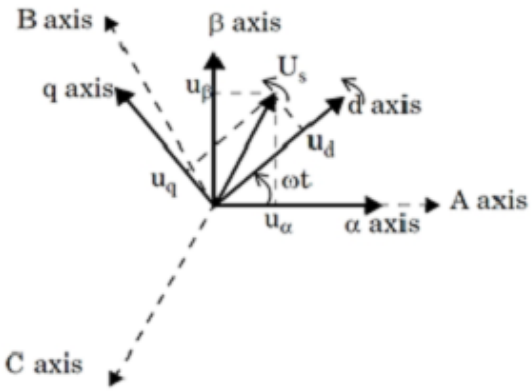

Fig. C.1: Reference Frames

$The\ \alpha\ -\ \beta\ Reference\ Frame$:

Clarke's Transformation helps us to simplify three phase variables into two phase variables. In order to transfer natural reference into $\alpha - \beta$ reference frame, following transformation is used,

$$\begin{bmatrix} i_\alpha \\ i_\beta \\ i_0 \end{bmatrix} = \sqrt{\frac{2}{3}} \begin{bmatrix} 1 & \frac{-1}{2} & \frac{-1}{2} \\ 0 & \frac{\sqrt{3}}{2} & \frac{-\sqrt{3}}{2} \\ \frac{1}{\sqrt{2}} & \frac{1}{\sqrt{2}} & \frac{1}{\sqrt{2}} \end{bmatrix} \begin{bmatrix} i_a \\ i_b \\ i_c \end{bmatrix}$$

$The\ d\ -\ q\ Reference\ Frame$:

Park's Transformation is similar to $\alpha - \beta$ transform but it has one advantage that it can be transformed into any arbitrary reference frame. In order to transfer natural reference into $d\ -\ q$ reference frame, following transformation is used. For $d\ -\ q$ variables in synchronous reference frame d-axis is aligned along A – axis. $d\ -\ q$ transform reduces complexity in controller design as the resultant phasor seen by the frame of reference is a DC quantity. $\begin{bmatrix} i_d \\ i_q \\ i_0 \end{bmatrix} = \sqrt{\frac{2}{3}} \begin{bmatrix} sin(\theta) & sin(\theta - 120) & sin(\theta + 120) \\ cos(\theta) & cos(\theta - 120) & cos(\theta + 120) \\ \frac{1}{\sqrt{2}} & \frac{1}{\sqrt{2}} & \frac{1}{\sqrt{2}} \end{bmatrix} \begin{bmatrix} i_a \\ i_b \\ i_c \end{bmatrix}$

Reference (Vasudevan, 2020)

APPENDIX D

The LC filter

The LC filter design for the inverter which using the Sinusoidal Pulse Width Modulation (SPWM) is imperative. This modulation method will produce a lot of harmonic in the switching frequency. In the real program, people always use the LC Passive power filter to solve this problem. (Mojgan Hojabri, 2015)

$$The\ formula\ of\ LC\ filter\ design\ is\ : \begin{cases} f_r\ = \frac{1}{2\ \pi\ \sqrt{L_f\ C_f}} \\ 10\ f_m\ \leq\ f_r\ \leq\ f_s/10 \end{cases}$$

where, f_r is the resonant frequency of LC filter, f_m is the frequency of modulating wave, and f_s is the frequency of SPWM carrier wave.

Finding values of L-C parameters :

for selection of capacitor,

Reactive power support (capacitive) = 5 % of rated power (S)

$Q = \frac{V^2}{(1/(2\ \pi\ f\ C_f))} = 5\ \%\ S$

thus, $C_f = \frac{0.005\ S}{(2\ \pi\ f\ )}$

once C_f is evaluated the L_f can be calculated using,

$L_f = \frac{1}{(2\ \pi\ C_f\ {f_r}^2)}$

APPENDIX E

MATLAB Code for Extracting Controller Parameters

```
%Frequencies
fs    = 10000;                                  % Switching frequency
Ts    = 1e-6;                                   % Sampling frequency
fc    = fs/10;                                  % Current controller
    frequency
fp    = fc/10;                                  % PQ controller
    frequency
f     = 50;                                     % Grid frequency

% Voltages
Vdc   = 800;                                    % Voltage at DC bus
Vrms  = ( 0.8 * Vdc ) / ( 2 * sqrt(2) );        % AC phase voltage
Vm    = sqrt(2) * Vrms;                         % Peak value of phase
    voltage

% Filter LR parameters
L     = 0.04;                                   % Filter inductance
R     = 1;                                      % Filter resistance

% PQ references
Pref  = 3e+3;                                   % Active power
    reference
Qref  = 222;                                    % Reactive power
    reference

%Current Controller Design
T_i   = 1 / ( 2 * pi * fc );                    % L/R time constant
Kp_i  = L / T_i;                                % Proportional constant
Ki_i  = R / T_i;                                % Integral constant

```

```
%PQ Controller Design
PM    = 70;                                    % Phase margin
wgc   = 2*3.14*fp;                             % Gain crossover
    frequency
ang   = atand(wgc*T_i) + PM - 90;              % Phase term numerator
t_p1  = sqrt( 1 + T_i * T_i * wgc * wgc );     % Gain term numerator
t_p2  = 1.5 * Vm;                              % Gain term denominator
Kp_pq = ( sind( ang ) * t_p1 ) / t_p2;         % Proportional constant
Ki_pq = ( wgc * cosd( ang ) * t_p1 ) / t_p2;   % Integral constant
```

REFERENCES

1. **Ashok Jhunjhunwala, L. K. P. K., Kaushal Kumar Jha** (2021). *Electric Vehicle and Renewable Energy System, a video course offered by NPTEL.* NPTEL, India.

2. **Blaabjerg, F.** (2018). *Control of Power Electronic Converters and Systems*. Elsevier Inc.

3. **Gao, W.** (2019). *Control Strategy for a Small-Scale Microgrid Based on Battery Energy Storage System Virtual Synchronous Generator (Bess-Vsg)"*. Electronic Theses and Dissertations,1659.

4. **Keyhani, A.** and **M. Marwali** (2011). *Smart Power Grids*. Springer-Verlag Berlin Heidelberg.

5. **Mojgan Hojabri, A. T., Mehrdad Hojabri** (2015). *Passive Damping Filter Design And Application For Three-Phase PV Grid-Connected Inverter*. International Journal of Electrical, Electronics and Data Communication, ISSN: 2320-2084.

6. **Patel, P. V.** (2018). *Modeling and control of three-phase grid-connected PV inverters in the presence of grid faults*. Masters Theses. 7806.

7. **Sattar, A.** (2016). *Insulated Gate Bipolar Transistor (IGBT) Basics*. XYS Corporation.

8. **Shen, Y.** (2017). *Microgrid Control Strategy Study and Controller Design Based on Model Predictive Control*. Electronic Theses and Dissertations,1241.

9. **Vasudevan, K.** (2020). *Modelling and Analysis Of Electrical Machine, a video course offered by NPTEL.* NPTEL, India.